

Coupled Bending-Twist Vibration of a Horizontal Axis Wind Turbine Blade Accounting for Tower Shadow Under Turbulent Flow

Paraskeva Maria

Technische Universiteit Delft



Coupled Bending-Twist Vibration of a Horizontal Axis Wind Turbine Blade Accounting for Tower Shadow Under Turbulent Flow

by

Paraskeva Maria

to obtain the degree of Master of Science
at Delft University of Technology,
to be defended publicly on Wednesday November 28th, 2018 at 14:00 PM.

Student number: 4621999
Project duration: November 20, 2017 - November 28, 2018
Supervisor: Prof. dr. A. V. Metrikine, Chair
Thesis committee: Ir. P. van derMale, TU Delft
Dr. ir. K. N. van Dalen, TU Delft
Ir. E. Vlijm, Witteveen+Bos

An electronic version of this thesis is available at <http://repository.tudelft.nl/>.

Correspondence with the author may be directed to
mariaparaskeva200392@gmail.com



Abstract

Due to global warming effect humanity is forced to seek cleaner forms of energy. One of these are renewable energies, which are inexhaustible and increasingly competitive. More specifically wind energy is of highly importance due to its benefits. In order to achieve ultimate wind energy exploitation, the design of wind turbines should be perfected. This rises a lot of challenges for engineering companies, which conduct research on more economically efficient and structurally reliable structures.

However, due to difficulties in modeling, industry turns into simpler ways of simulating the conditions and loads under which a wind turbine functions. This project aims at providing a simple yet precise model, which takes into account the aerodynamic interaction of a horizontal axis wind turbine blade. The blade is modeled using an Euler-Bernoulli beam and the cross section is considered to be symmetric, taking into account the coupled bending-twist vibration of the blade. The aerodynamic interaction depends on the relative wind velocity, which includes the vibrational velocity of the blade.

The main objective of this project is the tower shadow effect on the structural behavior of the blade. The tower is modeled using a mass attached to a stiffness spring, which are connected to the blade. The chosen mass and stiffness were tuned to the first bending mode of the tower so as to obtain its first fore-aft natural frequency. The tower effect on the natural frequencies of the blade is not as expected. Hence a simpler 2 DOF system was constructed to assess this behavior. By doing so, it is observed that the tower induces an extra vibration to the blade tip response which is also observed in the first mode of the system, which is a rigid body mode with initial displacement due to the existence of the spring.

The wind profile used was Kaimal Spectrum and the aerodynamic loading was simulated using instantaneous aerodynamics. The tower shadow velocity profile was created for two cases, an upwind and a downwind wind turbine. For the upwind case, the velocity profile was derived from the stream function around a cylindrical tower and for the downwind case Powles model was utilized. The study revealed that the downwind tower shadow has a bigger effect on the blade response. However, it should be noted that the turbulence close to the downwind edge of the tower has not been studied extensively in literature and as a result is has been roughly represented here. To better understand and model this effect more experiments should be conducted in the future.

Acknowledgements

This thesis finalizes my studies at Delft University of Technology for the acquisition of the Master of Science in Offshore and Dredging Engineering. This could not have been possible without the contribution of numerous people.

First and foremost I would like to thank all the members of the graduation committee. I would like to acknowledge and thank Professor dr. A. V. Metrikine for chairing this project and for his insightful questions that helped me improve my research. I am also extremely grateful to my supervisors for trusting me to participate in this project. Special thanks go to Ir. Pim van der Male for his guidance through the project and for the time he invested to give solutions to my questions or to discuss my thoughts on the research. I would also like to thank Ir. Eliam Vlijm for giving me the opportunity to conduct this project at Witteveen+Bos since it is quite important for me to start adapting to a corporate environment.

I would also like to thank my family and especially my parents, but most of all my little niece and my sister who I have tremendously missed during the previous year. Last but not least I would like to thank my boyfriend for being by my side in the good and bad moments during this journey.

*Paraskeva Maria
Delft, November 2018*

Contents

Abstract	i
Acknowledgements	ii
List of Figures	v
List of Tables	vii
1 Introduction	1
1.1 Renewable Energy	1
1.2 Problem Statement	2
1.3 Literature Review	2
1.4 Research Questions	3
1.5 Approach	3
1.6 Outline	4
2 Model Description	5
2.1 Equations of Motion	7
2.1.1 Transformation of coordinates	7
2.1.2 Definition of the Velocity Vector and deformation vector	8
2.1.3 Strain Energy and Kinetic Energy	9
2.1.4 Derivation of Equation of Motion	10
2.2 Equations of Motion Including the Tower	13
3 Finite Element Analysis	14
3.1 Beam Element	15
3.2 Discretization of the Blade	15
3.3 Stiffness and Mass Matrices	16
3.4 Assembling the Global Matrices	21
3.5 Validation	22
3.6 Introduction of the Tower	23
4 Eigenanalysis	24
4.1 Eigenvalues and Eigenmodes	24
4.1.1 Coupled bending twist vibration	24
4.1.2 Coupled vibration of a standstill and a rotating blade	25
4.1.3 Coupled bending twist vibration of the complete model	27
5 Aerodynamic Analysis	32
5.1 Instantaneous Aerodynamic Loading	33
5.2 Wind Spectrum	34
6 Results and Discussion	36
6.1 Steady Flow	37
6.1.1 Influence of gravity	37
6.1.2 Influence of Aerodynamic Interaction	40
6.2 Unsteady Flow	43
6.2.1 Influence of gravity	43
6.2.2 Influence of Aerodynamic Interaction	46
6.3 Tower Shadow Effect	49
6.3.1 Steady Flow	52
6.3.2 Unsteady Flow	55

7	Conclusions and Recommendations	57
7.1	Conclusions	57
7.2	Recommendations	58
	Bibliography	59

List of Figures

2.1	Position of the COM with respect to pitch center, aerodynamic center, shear center and tension center	6
2.2	Degrees of freedom of the blade	6
2.3	Azimuth angle of the rotor	7
2.4	Pitching of the blade	7
2.5	Torsion of the blade	8
2.6	Model Including Tower	13
3.1	Degrees of freedom applied to a beam element	15
3.2	Discretization of the Blade	20
3.3	Local Configuration of the nodal DOFs	21
3.4	Global Configuration of the nodal DOFs	21
3.5	Assembled Global Configuration of the nodal DOFs	22
4.1	Eigenmodes of a standstill Blade	26
4.2	Simple 2 DOF system	27
4.3	Natural Frequencies of 2DOF system	28
4.4	Natural Frequencies of complete model	29
4.5	Eigenmodes of the complete model	30
5.1	Aerodynamic Configuration with the definition of the angle of attack and definition of drag and lift forces	33
5.2	Kaimal Turbulence Spectrum in the longitudinal and lateral direction and the wind velocity fluctuation around the mean	35
6.1	Influence of gravity on a rotating blade accounting both aerodynamic interaction and gravity	37
6.2	Influence of gravity on a rotating blade accounting only the aerodynamic interaction	37
6.3	Influence of gravity on a standstill blade accounting both the aerodynamic interaction and the gravity	38
6.4	Influence of gravity on a rotating blade with tower a) and b) taking into account both gravity and aerodynamic interaction, while c) and d) represent the same but without considering gravity	39
6.5	Influence of aerodynamic interaction on a rotating blade accounting only the gravity	40
6.6	Influence of aerodynamic interaction on a standstill blade accounting only the gravity	40
6.7	Influence of aerodynamic interaction on a rotating blade with tower taking into account only gravity	41
6.8	Effect of tower on blade tip response -comparison between the cases with/without tower considering only gravity (blue and red line)- comparison between the cases with/without tower considering both gravity and aerodynamic interaction (yellow and purple line)	42
6.9	Influence of gravity on a rotating blade a) and b) taking into account both gravity and aerodynamic interaction, while c) and d) represent the same but without considering gravity	43
6.10	Influence of gravity on a standstill blade accounting both the aerodynamic interaction and gravity	44

6.11 Influence of gravity on a rotating blade with tower a) and b) taking into account both gravity and aerodynamic interaction, while c) and d) represent the same but without considering gravity	45
6.12 Influence of aerodynamic interaction on a rotating blade a) and b) taking into account both gravity and aerodynamic interaction, while c) and d) represent the same but without considering the aerodynamic interaction	46
6.13 Influence of aerodynamic interaction on a standstill blade a) and b) taking into account both gravity and aerodynamic interaction, while c) and d) represent the same but without considering the aerodynamic interaction	47
6.14 Influence of aerodynamic interaction on a rotating blade with tower taking into account only gravity	48
6.15 Tower Shadow Parameters according to [25]	50
6.16 Velocity Profile due to Tower Shadow-Upwind versus Downwind case	51
6.17 Blade tip response without aerodynamic interaction considering gravity a) and b) upwind tower shadow effect while c) and d) represent the same but considering downwind tower shadow effect	52
6.18 Blade tip response considering both aerodynamic interaction and gravity a) and b) upwind tower shadow effect while c) and d) represent the same but considering downwind tower shadow effect	53
6.19 Influence of tower shadow a) on a rotating blade with tower taking into account only gravity b) on a rotating blade with tower considering both aerodynamic interaction and gravity	54
6.20 Blade tip response without aerodynamic interaction considering gravity a) and b) upwind tower shadow effect while c) and d) represent the same but considering downwind tower shadow effect	55
6.21 Blade tip response considering both aerodynamic interaction and gravity a) and b) upwind tower shadow effect while c) and d) represent the same but considering downwind tower shadow effect	56

List of Tables

3.1 Comparison of the natural frequencies	22
4.1 Coupled Model	25
4.2 Standstill versus rotating blade	25
4.3 natural frequencies of the complete model	27
4.4 natural frequencies of the complete model	27
6.1 Operating Conditions of the wind turbine	36

Introduction

1.1. Renewable Energy

Due to global warming effect humanity was forced to seek cleaner forms of energy. One of them are renewable energies, which are clean, inexhaustible and increasingly competitive. They differ from fossil fuels principally in their diversity, abundance and potential for use anywhere on the planet, but above all in that they produce neither greenhouse gases – which cause climate change – nor polluting emissions. Their costs are also falling and at a sustainable rate, whereas the general cost trend for fossil fuels is in the opposite direction in spite of their present volatility.

Growth in clean energies is unstoppable, as reflected in statistics produced in 2015 by the International Energy Agency (IEA): they represented nearly half of all new electricity generation capacity installed in 2014, when they constituted the second biggest source of electricity worldwide, behind coal.

According to the IEA, world electricity demand will have increased by 70% by 2040 - its share of final energy use rising from 18 to 24% during the same period – driven mainly by the emerging economies of India, China, Africa, the Middle East and South-East Asia.

Renewable energies include:

- Wind energy: the energy obtained from the wind
- Solar energy: the energy obtained from the sun. The main technologies here are solar photovoltaic (using the light from the sun) and solar thermal (using the sun's heat)
- Hydraulic or hydroelectric energy: energy obtained from rivers and other freshwater currents
- Biomass and biogas: energy extracted from organic material
- Geothermal energy: heat energy from inside the Earth
- Tidal energy: energy obtained from the tides
- Wave energy: energy obtained from ocean waves
- Bioethanol: organic fuel suitable for vehicles and obtained from fermentation of vegetation
- Biodiesel: organic fuel for vehicles, among other applications, obtained from vegetable oils

From the above wind energy is of highly importance due to its benefits. It does not contaminate, it is inexhaustible and reduces the use of fossil fuels, which are the origin of greenhouse gasses that cause global warming. In addition, wind energy is a “native” energy, because it is

available practically everywhere on the planet. It reduces energy imports and creates wealth and local employment. In addition, wind energy does not emit toxic substances or contaminants into the air, which can be very damaging to the environment and to human beings. Toxic substances can acidify land and water ecosystems, and corrode buildings. Air contaminants can trigger heart disease, cancer and respiratory diseases like asthma. Also it does not generate waste or contaminate water, an extremely important factor given the scarcity of water. Unlike fossil fuels and nuclear power plants, wind energy has one of the lowest water-consumption footprints, which makes it a key for conserving hydrological resources.

In order to achieve ultimate wind energy exploitation the design of wind turbines should be perfected. This rises a lot of challenges for engineering companies which conduct research on more efficient economically and structurally reliable structures. However, due to difficulties in modeling, companies turn into simpler ways of simulating the conditions and loads, under which a wind turbine functions. Some of these difficulties are analyzed in the next sections.

1.2. Problem Statement

In the preliminary design of a wind turbine there is no need for a complete model of the structure. As a result, since we are interested in the aerodynamic interaction of a Horizontal Axis wind turbine, a simplified model of the hub and one blade, fixed to the hub is used. However, at later stages in this study, in order to be more precise, the tower will be modeled using one stiffness spring and a mass attached to the spring. In order to compare the two models, their natural frequencies will be compared and the effect of the tower on the blade will be assessed. The main purpose of this project is to examine the interference of the tower with the blade under aerodynamic forcing. In addition, the load due to the Tower Shadow will be modeled for upwind and downwind case and the effect of the tower shadow will be observed on the blade tip response, taking into consideration steady and turbulent flow.

The challenges faced during the above analysis are numerous. First of all the formulation of equations of motion should be precise and accurate in order to represent correctly the motion of the system. In addition, as far as the aerodynamic loading is concerned there is damping and added mass due to the aerodynamic interaction of the structure with the wind, which should be taken into account and two cases were considered: a steady and an unsteady (turbulent) scenario. The aerodynamic interaction depends also on the relative wind velocity experienced by the blade. Another challenge was the fact that the blade undergoes two different states of operation. More specifically when the blade is 'pitched on' it does not rotate and when it is 'pitched off' it operates. The rotation of the blade results in a centrifugal force which induces a stiffening effect to the blade, called 'centrifugal stiffening' along the axial direction. Also gravity needs to be taken into account as it induces a harmonic loading to the blade, affecting the blade response. A challenging part was also the effect of the tower on the blade, as the results were not as expected, as far as the natural frequencies are concerned and various cases were analyzed in order to assess the accuracy of the results. Finally, an upwind and a downwind case for tower shadow were modeled.

1.3. Literature Review

The initial model used is studied by Van der Male *et al* [3] in which the blade is modeled by a twisted rotating Euler Bernoulli beam fixed to a rigid hub. In this specific case the torsion of the blade and the gravity are ignored. The coupled bending-twist vibration of the blade is accounted for by Houbolt & Brooks [4] and Hodges & Dowell [2] but still the effect of gravity is not included. Kallesøe [1] included torsion and gravity but without taking into account the interaction with the aerodynamic loading. G. Surace *et al* [6] also conducted an analysis on the coupled bending-torsion vibration of a pretwisted blade but restricted only to the modal characteristics of the blade. S. M. Lin *et al* [7] conducted a vibrational analysis of a pretwisted beam with tip mass ignoring torsion. Similarly, H. Kim *et al* [20] ignored torsion in their research. In addition, a common characteristic of all the above researches is that none of these observed how the aerodynamic load would affect the blade when considering the tower, which is of highly importance.

The present project accounts for more realistic conditions of functioning for the wind

turbine such as aerodynamic interaction, gravity, coupled bending twist vibration and tower shadow.

As mentioned before in the preliminary design of a wind turbine the complete model of the structure is not a necessity. However, in order to conduct a precise and effective dynamic analysis of a wind turbine, an experimental and a theoretical modal analysis should be conducted. The present project deals with the theoretical part of the dynamic analysis, but it aims to contribute also in the experimental part of it. In order to avoid the rising limitations in large scale experiments of wind turbines, the theoretical analysis needs constant improvement in order to be so precise that the need of experimental analysis could be possibly eliminated in the future.

In conventional design analysis the wind turbine is modeled by lumping the mass of the components (nacelle, rotor, and blades) at the top of the tower. However, not much published literature exists to illustrate the interaction between the motion of the blades and the tower, which is studied in this specific project. Wang et al [21] model the tower as an Euler- Bernoulli beam attached to a lumped mass which consists of the mass of blade-rotor-gearbox-generator with only two degrees of freedom, investigating the interaction between the nacelle-tower-foundation and stating that this simplified model is adequate in case of incomplete structural properties.

Kang et al [22] modeled the wind turbine by two beams, one for the tower and one for the blade attached to each other. Each beam has only one bending degree of freedom on the fore-aft direction. Kessentini et al [23] use a detailed model of the wind turbine including the tower as a beam and considering three blades but only the flapwise deflection of each blade is considered and rotation is ignored. In addition, none of the above research includes aerodynamic analyses on the complete model. This project comes to fill this gap of knowledge by expanding the research on the aerodynamics of the model.

As far as the tower shadow around a tubular tower is concerned [26] and [27] have studied and analyzed the flow around the tower using various tower shadow models. However their research did not expand on the effect of the tower shadow on the blade. In addition to that the characteristics of tower shadow as velocity deficit or wake length were considered based on experiments or empirical data. In this project the consequences of the tower shadow effect are illustrated for different flow conditions.

1.4. Research Questions

In order to analyze the problems explained previously the following research questions were formed:

- What is the effect of the tower on the structural behavior of the blade?
- How does the tower affect the blade response?
- How does the tower shadow effect influence the blade response?
- Which type of tower shadow (upwind vs downwind) is more significant?.

1.5. Approach

The approach followed in the present project consists of the following steps:

1. Formulation of equations of motion including torsion, bending and gravity
2. Formulation of aerodynamic loading equations
3. Aerodynamic analysis considering different conditions mentioned previously.
4. Introduction of upwind and downwind tower shadow velocity profiles
5. Comparison of Results

After following these steps the model is analyzed using MATLAB and the different cases are compared.

1.6. Outline

The thesis is outlined as follows. Chapter 2 describes the equations of motion of the system, including the tower. Continuously the system is discretized into finite elements in chapter 3 and after analyzing the finite element system, its eigenmodes are presented in chapter 4. The aerodynamic loads are then defined in chapter 5 and the results are illustrated and analyzed in chapter 6. Finally, conclusions and recommendations are presented in chapter 7.

2

Model Description

This chapter illustrates the transformation matrices between the different coordinate frames and the equations of motion. The aim of this, is to create a solid base for the finite element method in order to carry out the eigenanalysis.

The motions of the blade are flapwise bending with respect to y axis, edgewise bending with respect to z axis and torsion with respect to r axis, as it is obvious in figure 2.2. In order to obtain the equations of motion, four coordinate frames are used according to [1][2][4]. These frames are the global fixed inertia reference frame (X, Y, Z), the global rotating reference frame (\tilde{r} , \tilde{y} , \tilde{z}), the local cross sectional frame (r, y, z) due to pitching and pre-twist and the local principal axis (ξ , η , ζ) due to torsion. The equations of motion are formulated in the global rotating reference frame as later on the aerodynamic loading will be applied on the blade in this frame.

During the derivation of the equations, according to [1],[2],[4], [8], [9], [10] some terms considering the blade are used which are clarified below.

1. Aerodynamic Centre: the point on the blade about which the aerodynamically generated moment is independent of the angle of attack.
2. Tension centre: The axis along the blade where an axial force applied along this axis does not introduce any bending moment across its cross-section. Also known as area centroid of the blade's cross-section.
3. Shear Centre: is the point where a lateral force will not rotate the aerofoil. It is also referred as the elastic axis of the blade.
4. Pitch center: The axis along the blade about which the blade is pitched.
5. Mass center: Also known as center of mass (COM) axis or gravity center of the cross-section and is defined as the point at any cross-section of the blade where the mass of that section is assumed to be concentrated.

During the analysis, the characteristics of the National Renewable Energy Laboratory (NREL) 5 MW turbine were adopted. According to [8] the pitch center is defined at the quarter chord point from the leading edge of the airfoil and it is assumed to coincide with the aerodynamic center. Generally during the present project the shear center, the pitch center, the aerodynamic center and the tension center are assumed to coincide according to [2],[4]. As far as the center of mass (COM) is concerned it is positioned at a varying distance $e(r)$ with respect to the chord length, away from the pitch center. The configuration of the above mentioned axes is represented on Figure 2.1.

In Figure 2.2 the blade undergoes flapwise bending $u(r,t)$, edgewise bending $v(r,t)$ and torsion $\varphi(r,t)$ around the elastic axis. Ω is the rotational velocity of the blade which is equivalent to the time derivative of the blade azimuth angle Ψ (illustrated in Figure 2.3).

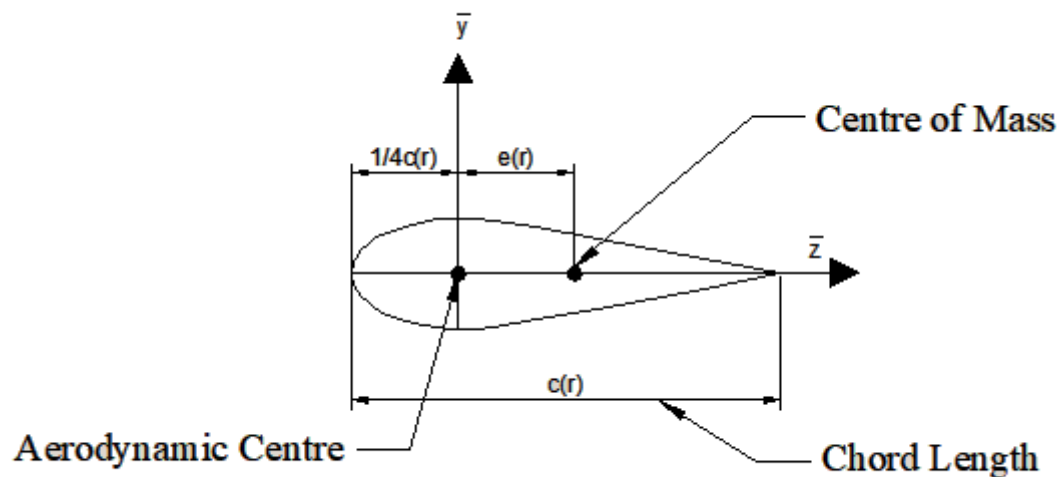


Figure 2.1: Position of the COM with respect to pitch center, aerodynamic center, shear center and tension center

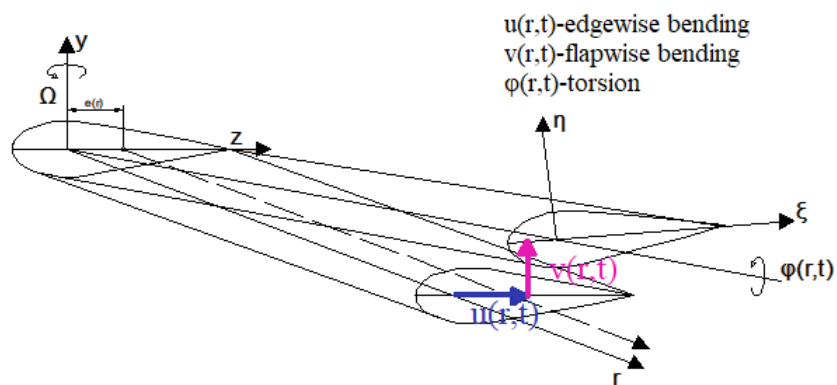


Figure 2.2: Degrees of freedom of the blade

In addition to the above it is worth mentioning that only one blade is taken into account. As a result the effect of vortex shedding from the rest of the blades is not taken into account. Some further assumptions that will be considered during the present project are:

1. Precone angle of the rotor is assumed to be zero.
2. No degrees of freedom are taken into account in the longitudinal direction of the blade
3. Attached flow is considered
4. Euler-Bernoulli beam theory is considered

2.1. Equations of Motion

Since the model requires four different coordinate frames it is important to derive the transformation matrices between them in order to relate them as the transverse deflections of the blade are defined in the global rotating reference frame \tilde{r} , \tilde{y} , \tilde{z} , whereas the torsion of the blade is defined in the local principal axis ξ , η , ζ .

2.1.1. Transformation of coordinates

Transformation from $\mathbf{X}, \mathbf{Y}, \mathbf{Z}$ to $\tilde{r}, \tilde{y}, \tilde{z}$ frame

The transformation incorporates the blade azimuth angle $\psi(t)$ according to [1] which is depicted in Figure 2.3.

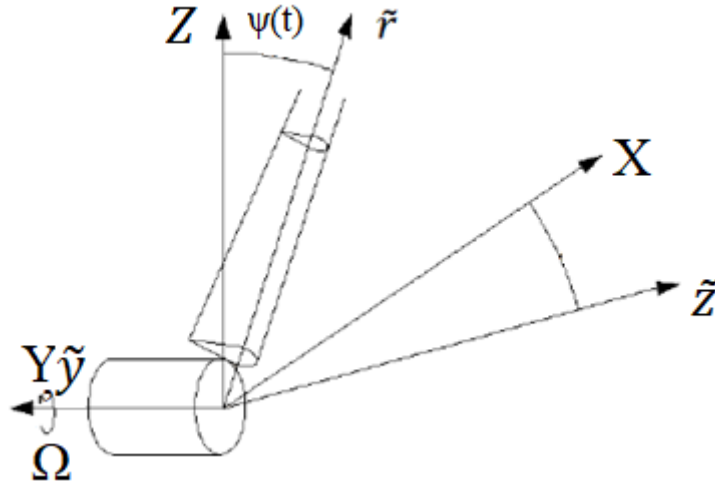


Figure 2.3: Azimuth angle of the rotor

$$\begin{bmatrix} \tilde{e}_r \\ \tilde{e}_y \\ \tilde{e}_z \end{bmatrix} = T_\psi \begin{bmatrix} e_x \\ e_y \\ e_z \end{bmatrix} = \begin{bmatrix} \sin \psi(t) & 0 & \cos \psi(t) \\ 0 & 1 & 0 \\ \cos \psi(t) & 0 & -\sin \psi(t) \end{bmatrix} \begin{bmatrix} e_x \\ e_y \\ e_z \end{bmatrix} \quad (2.1)$$

Transformation from $\tilde{r}, \tilde{y}, \tilde{z}$ to $\mathbf{r}, \mathbf{y}, \mathbf{z}$ frame

Afterwards due to pitching and pre-twist $\beta(r)$ as depicted in Figure 2.4 a modification takes place from the global rotating frame to the local cross sectional reference frame.

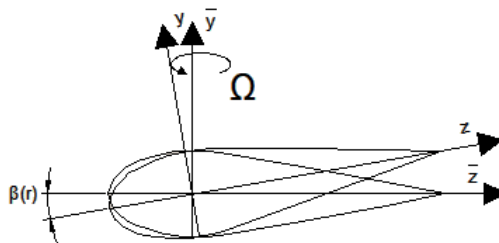


Figure 2.4: Pitching of the blade

$$\begin{bmatrix} e_r \\ e_y \\ e_z \end{bmatrix} = T_\beta \begin{bmatrix} \tilde{e}_r \\ \tilde{e}_y \\ \tilde{e}_z \end{bmatrix} = \begin{bmatrix} 1 & 0 & 0 \\ 0 & \cos \beta(r) & -\sin \beta(r) \\ 0 & \sin \beta(r) & \cos \beta(r) \end{bmatrix} \begin{bmatrix} \tilde{e}_r \\ \tilde{e}_y \\ \tilde{e}_z \end{bmatrix} \quad (2.2)$$

Transformation from r, y, z to ξ, η, ζ frame

Finally due to the torsion of the blade the transformation will take place from the local cross-sectional reference frame r, y, z . to the local principal axis ξ, η, ζ .

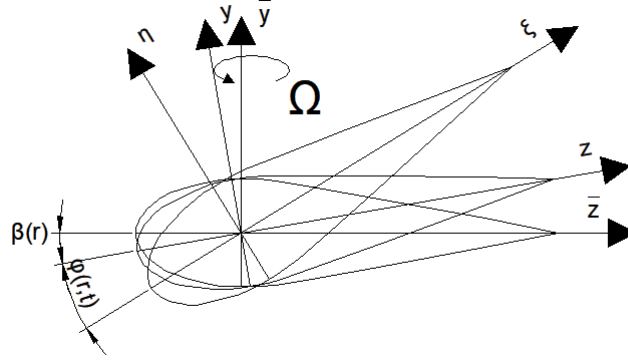


Figure 2.5: Torsion of the blade

$$\begin{bmatrix} \xi \\ \eta \\ \zeta \end{bmatrix} = \mathbf{T}_\phi \begin{bmatrix} e_r \\ e_y \\ e_z \end{bmatrix} = \begin{bmatrix} 1 & 0 & 0 \\ 0 & \cos\phi(r, t) & -\sin\phi(r, t) \\ 0 & \sin\phi(r, t) & \cos\phi(r, t) \end{bmatrix} \begin{bmatrix} e_r \\ e_y \\ e_z \end{bmatrix} \quad (2.3)$$

As the angle ϕ is really small according to [4] the transformation matrix takes the following form.

$$\begin{bmatrix} \xi \\ \eta \\ \zeta \end{bmatrix} = \mathbf{T}_\phi \begin{bmatrix} e_r \\ e_y \\ e_z \end{bmatrix} = \begin{bmatrix} 1 & 0 & 0 \\ 0 & 1 & -\phi(r, t) \\ 0 & \phi(r, t) & 1 \end{bmatrix} \begin{bmatrix} e_r \\ e_y \\ e_z \end{bmatrix} \quad (2.4)$$

2.1.2. Definition of the Velocity Vector and deformation vector

In order to derive the Lagrangian function two deformation vectors are needed. The deformation vector of the elastic axis as it is used in the derivation of the elastic strain energy and the deformation vector of the center of mass as it is used in the derivation of the kinetic energy and in the description of the geometric strain energy due to the centrifugal force according to [11].

The deformed position vector of the elastic axis in the global rotating frame $\tilde{r}, \tilde{y}, \tilde{z}$ is:

$$\mathbf{u}_{ea}(r, t) = \begin{bmatrix} \tilde{r} \\ v(r, t) \\ u(r, t) \end{bmatrix} \quad (2.5)$$

Using the transformation coordinate matrices 2.2 and 2.4 the deformed position vector of the center of mass in the global rotating reference frame axis in the global rotating frame $\tilde{r}, \tilde{y}, \tilde{z}$ according to [1] and [2] is:

$$\mathbf{u}(r, t) = \begin{bmatrix} \tilde{r} \\ u_y(r, t) \\ u_x(r, t) \end{bmatrix} = \mathbf{u}_{ea}(r, t) + \mathbf{T}_\beta^T \mathbf{T}_\phi^T \begin{bmatrix} 0 \\ 0 \\ e(r) \end{bmatrix} = \begin{bmatrix} \tilde{r} \\ v(r, t) + (\cos(\beta(r))\phi(r, t) + \sin(\beta(r)))e(r) \\ u(r, t) + (\cos(\beta(r)) - \sin(\beta(r))\phi(r, t))e(r) \end{bmatrix} \quad (2.6)$$

Since the blade exhibits degrees of freedom also in the lateral direction and the elastic axis the deformation vector of the center of mass will be:

$$\mathbf{u}_{cg}(r, t) = \begin{bmatrix} \phi(r, t) \\ u_y(r, t) \\ u_x(r, t) \end{bmatrix} = \begin{bmatrix} \phi(r, t) \\ v(r, t) + (\cos(\beta(r))\phi(r, t) + \sin(\beta(r)))e(r) \\ u(r, t) + (\cos(\beta(r)) - \sin(\beta(r))\phi(r, t))e(r) \end{bmatrix} \quad (2.7)$$

Similarly the deformation vector of the elastic axis will be:

$$\mathbf{u}_b(r, t) = \begin{bmatrix} \phi(r, t) \\ v(r, t) \\ u(r, t) \end{bmatrix} \quad (2.8)$$

In order to derive the velocity vector of the blade both the rotational velocity of the blade and the vibrational velocity of the center of mass will be taken into account similarly to [1][2].

$$\mathbf{V}(r, t) = \boldsymbol{\Omega} \times \mathbf{u}(r, t) + \dot{\mathbf{u}}(r, t) = \begin{bmatrix} 0 \\ \Omega \\ 0 \end{bmatrix} \times \mathbf{u}(r, t) + \dot{\mathbf{u}} = \begin{bmatrix} \Omega(u(r, t) + (\cos(\beta(r)) - \sin(\beta(r))\phi(r, t))e(r)) \\ \dot{v}(r, t) + \cos(\beta(r))\dot{\phi}(r, t)e(r) \\ -\Omega r + \dot{u}(r, t) - \sin(\beta(r))\dot{\phi}(r, t)e(r) \end{bmatrix} \quad (2.9)$$

Where $\boldsymbol{\Omega} \times \mathbf{u}(r, t)$ is the velocity of the blade due to its rotation and $\dot{\mathbf{u}}$ is the velocity due to the vibration of the blade.

2.1.3. Strain Energy and Kinetic Energy

Strain Energy

The strain energy of the system is the energy stored by the system when it undergoes a deformation [10]. In this specific case the potential energy consists of the energy due to potential difference according to [1], the elastic strain energy due to transverse and torsional deformation of the blade and the geometric strain energy due to centrifugal force [11].

$$U(t) = \int_{r_0}^R (\mathbf{G}^T \mathbf{M}(r) \mathbf{H} + \frac{1}{2} \mathbf{u}_b''(r, t)^T \mathbf{K}(r) \mathbf{u}_b''(r, t) + \frac{1}{2} \mathbf{u}_{cg}'(r, t)^T \mathbf{P}(r) \mathbf{u}_{cg}'(r, t)) dr \quad (2.10)$$

In the expression above the first term expresses the energy due to potential difference (assuming zero potential at the hub height). The gravity vector \mathbf{G} is expressed as:

$$\mathbf{G}^T = [0 \quad 0 \quad -g] \quad (2.11)$$

Where g is the acceleration of gravity. In addition, $\mathbf{M}(r)$ is the diagonal mass matrix and \mathbf{H} is the deformed position vector of the center of mass in the global fixed inertia reference frame.

$$\mathbf{H} = \mathbf{T}_\psi^T \mathbf{u}(r, t) \quad (2.12)$$

The second term of the equation corresponds to the elastic strain energy due to the blade bending and torsion in which $\mathbf{K}(r)$ is equal to:

$$\mathbf{K}(r) = \begin{bmatrix} GJ(r) & 0 & 0 \\ 0 & EI_{yy}(r) & EI_{xy}(r) \\ 0 & EI_{xy}(r) & EI_{xx}(r) \end{bmatrix} \quad (2.13)$$

Since the blade deformation is defined at the elastic axis, the stiffness matrix is uncoupled between bending and torsion.

The third term represents the geometric strain energy due to the centrifugal force. This term expresses the work that needs to be done by the centrifugal force to restore the beam to its initial position. This term is analytically explained in [12]. The centrifugal force due to the rotation of the blade around the hub and the axial gravitational force is equal to:

$$Tn(r) = \Omega^2 \int_{r_0}^R m(r)r dr - \cos(\psi(t))g \int_{r_0}^R m(r) dr \quad (2.14)$$

Where R is the length of the blade.

The axial gravitational force needs to be included because as the blade rotates it experiences either a compressive or a tensile force depending on its position. As a result $\mathbf{P}(r)$ is equal to:

$$\mathbf{P}(r) = \begin{bmatrix} 0 & 0 & 0 \\ 0 & Tn(r) & 0 \\ 0 & 0 & Tn(r) \end{bmatrix} \quad (2.15)$$

Kinetic Energy

Kinetic energy, is the energy obtained by the system due to its motion. The expression of it is:

$$T(t) = \int_{r_0}^R \left(\frac{1}{2} \mathbf{V}^T(r,t) \mathbf{M}(r) \mathbf{V}(r,t) + \frac{1}{2} J_{cg}(r) \dot{\phi}(r,t)^2 \right) dr \quad (2.16)$$

In the above expression the kinetic energy due to the translational motion of the blade and the kinetic energy due to the torsional motion are included. J_{cg} is the mass moment of inertia of the blade cross section around the center of mass .

2.1.4. Derivation of Equation of Motion

In order to derive the equations of motion the variational approach is used, which includes the use of Hamilton's principle. This method is more efficient than the Newtonian method for continuous systems as it avoids working with extra unknowns resulting from the equilibrium equations of each discrete mass.

Hamilton's principle makes use of the Lagrangian density function:

$$\hat{L}(t) = \hat{T}(t) - \hat{U}(t) \quad (2.17)$$

In the above equation \hat{T} and \hat{U} are the kinetic and strain energy densities respectively and they are equal to:

$$T(t) = \int_{r_0}^R \hat{T}(t) dr \quad (2.18)$$

$$U(t) = \int_{r_0}^R \hat{U}(t) dr \quad (2.19)$$

Using the above expressions the equation of motion can be derived using Hamilton's principle :

$$\frac{\partial \hat{L}(r,t)}{\partial \mathbf{u}_b(r,t)} - \frac{\partial}{\partial r} \frac{\partial \hat{L}(r,t)}{\partial \mathbf{u}_b'(r,t)} + \frac{\partial}{\partial r^2} \frac{\partial \hat{L}(r,t)}{\partial \mathbf{u}_b''(r,t)} - \frac{\partial}{\partial t} \frac{\partial \hat{L}(r,t)}{\partial \dot{\mathbf{u}}_b(r,t)} = 0 \quad (2.20)$$

The derivation of the above formula is well illustrated in [12] and [13].

Hamilton's equation of motion in $\mathbf{u}(r,t)$

The equation of motion in $\mathbf{u}(r,t)$ is expressed as :

$$(EI_{xx}u''(r,t) + EI_{xy}v''(r,t))'' = p_x \quad (2.21)$$

in which p_x is equal to :

$$\begin{aligned} p_x = & m(r)\Omega^2(u(r,t) + \cos(\beta(r))e(r) - \phi(r,t)e(r)\sin(\beta(r))) \\ & + \{Tn(r)(u(r,t) + \cos(\beta(r))e(r) - \phi(r,t)\sin(\beta(r))e(r))\}' \\ & + m(r)(\sin(\beta(r))e(r)\ddot{\phi}(r,t) - \ddot{u}(r,t)) - gm(r)\sin(\psi(t)) \end{aligned} \quad (2.22)$$

According to equation 2.7:

$$p_x = m(r)\Omega^2u_x(r,t) + \{Tn(r)u_x'(r,t)\}' - m(r)\ddot{u}_x(r,t) - gm(r)\sin(\psi(t)) \quad (2.23)$$

With respect to equation 2.23 the first term represents the centrifugal force due to the rotation of the blade and the position of the center of mass. The second term, and especially the term in brackets represents the shear force associated with the axial force and the blade deflection. The derivative of the term in brackets expresses a distributed force in the x-direction, introduced by the axial force and the blade deflection. The third term represents the force due to the motion of the center of mass and the fourth term represents the applied force to the blade due to the acceleration of gravity.

The boundary conditions according to Hamilton are the following:
At $r = r_0$

$$\begin{aligned} u(r_0, t) &= 0 \\ \frac{\partial u(r, t)}{\partial r} \Big|_{r=r_0} &= 0 \end{aligned} \quad (2.24)$$

The above equations represent that the deflection and the slope of the blade at the fixed end of the blade will be equal to zero.

At $r = R$

$$(EI_{xx}u''(r, t) + EI_{xy}v''(r, t))|_{r=R} = 0 \quad (2.25)$$

$$\begin{aligned} \{Tn(r)(u(r, t) + \cos(\beta(r))e(r) - \phi(r, t)\sin(\beta(r))e(r))\}' - \\ (EI_{xx}u'''(r, t) + EI_{xy}v'''(r, t))|_{r=R} = 0 \end{aligned} \quad (2.26)$$

Hamilton's equation of motion in $\mathbf{v}(r, t)$

The equation of motion in $\mathbf{v}(r, t)$ is expressed as :

$$(EI_{yy}v''(r, t) + EI_{xy}u''(r, t))'' = p_y \quad (2.27)$$

in which p_y is equal to :

$$\begin{aligned} p_y = \{Tn(r)(v(r, t) + \cos(\beta(r))\phi(r, t)e(r) + \sin(\beta(r))e(r))\}' - \\ -m(r)(\cos(\beta(r))e(r)\ddot{\phi}(r, t) + \ddot{v}(r, t)) \end{aligned} \quad (2.28)$$

According to equation 2.7:

$$p_y = \{Tn(r)u_y'(r, t)\}' - m(r)\ddot{u}_y(r, t) \quad (2.29)$$

The terms of equation 2.29 can be interpreted similarly to the terms of equation 2.23. However in that specific case there is no centrifugal force because it does not act in that direction. In addition the gravitational force is also not applied in that direction.

The boundary conditions according to Hamilton are the following:

At $r = r_0$

$$\begin{aligned} v(r_0, t) &= 0 \\ \frac{\partial v(r, t)}{\partial r} \Big|_{r=r_0} &= 0 \end{aligned} \quad (2.30)$$

The above equations represent the deflection and the slope of the blade at the fixed end of the blade.

At $r = R$

$$(EI_{yy}v''(r, t) + EI_{xy}u''(r, t))|_{r=R} = 0 \quad (2.31)$$

$$\begin{aligned} \{Tn(r)(v(r, t) + \cos(\beta(r))\phi(r, t)e(r) + \sin(\beta(r))e(r))\}' - \\ (EI_{yy}v'''(r, t) + EI_{xy}u'''(r, t))|_{r=R} = 0 \end{aligned} \quad (2.32)$$

The above equations represent the bending moment and the shear force at the free end of the blade.

Hamilton's equation of motion in $\phi(r, t)$

The equation of motion in $\phi(r, t)$ is expressed as:

$$(GJ\phi'(r, t))' + p_r = 0 \quad (2.33)$$

In the case of torsion it needs to be considered that the potential energy according to [14] is equal to :

$$U = \frac{1}{2} \int_{r_0}^R GJ(\phi'(r, t))^2 dr \quad (2.34)$$

As a result for this specific case the total potential energy will be redefined as:

$$U(t) = \int_{r_0}^R (\mathbf{G}^T \mathbf{M}(r) \mathbf{H} + \frac{1}{2} GJ(\phi'(r, t))^2 + \frac{1}{2} \mathbf{u}_{cg}'(r, t)^T \mathbf{P}(r) \mathbf{u}_{cg}'(r, t)) dr \quad (2.35)$$

Using the above expression p_r is equal to :

$$\begin{aligned} p_r = & -m(r)e(r)\Omega^2 u(r, t)\sin(\beta(r)) + e(r)m(r)g\sin(\psi(t))\sin(\beta(r)) \\ & m(r)e(r)^2\Omega^2(-\cos(\beta(r))\sin(\beta(r)) + \sin^2(\beta(r))\phi(r, t)) \\ & m(r)e(r)(-\cos(\beta(r))\ddot{v}(r, t) + \sin(\beta(r))\ddot{u}(r, t)) - \\ & (e(r)^2m(r) + J_{cg})\ddot{\phi}(r, t) + (e(r)^2Tn(r)\phi'(r, t))' + (\beta'(r)e(r)^2Tn(r))' \\ & + \phi(r, t)(Tn(r)e'(r))'e(r) - \phi(r, t)(\beta'(r))^2e(r)^2Tn(r) \\ & Tn(r)e(r)(-\sin(\beta(r))u''(r, t) + \cos(\beta(r))v''(r, t)) \\ & Tn'(r)e(r)(-\sin(\beta(r))u'(r, t) + \cos(\beta(r))v'(r, t)) \end{aligned} \quad (2.36)$$

In equation 2.36 the derived terms are multiple and complicated. Therefore some of them will be interpreted. One important term is the term in the beginning of the fourth line $(e(r)^2m(r) + J_{cg})\ddot{\phi}(r, t)$ which represents the torque due to the torsional acceleration . In addition to this the second term in the first line represents the torque due to the eccentricity of the gravitational force. The second and third term in the fourth line illustrate the torque introduced from the torsion and the pre-twist of the blade correspondingly.

The boundary conditions according to Hamilton's principle are:

At $r = r_0$

$$\phi(r_0, t) = 0 \quad (2.37)$$

At $r = R$

$$\begin{aligned} & (GJ\phi'(r, t) + Tn(r)e(r)(-\sin(\beta(r))u'(r, t) + \cos(\beta(r))v'(r, t)) + \\ & \beta'(r)e(r)^2Tn(r) + \phi'(r, t)e(r)^2Tn(r) + \phi(r, t)Tn(r)e'(r))|_{r=R} = 0 \end{aligned} \quad (2.38)$$

Equation 2.37 and 2.38 represent correspondingly the twist angle at the fixed end of the blade and the torque at the free end.

2.2. Equations of Motion Including the Tower

In this specific project the tower is modeled by using a stiffness spring and a mass connected to it as it is obvious in 2.6.

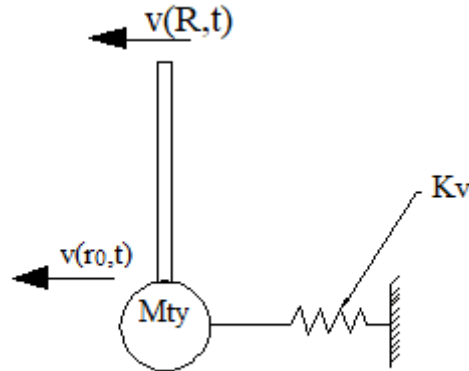


Figure 2.6: Model Including Tower

In the above figure the mass of the tower is illustrated by the quantity M_{ty} and the displacement of the tower is equal to the displacement of the blade at the point where it connects to the tower which is illustrated by $v(r_0, t)$. The equations of motion of the blade will remain the same as the were stated in sub chapter 2.1.4.

The kinetic energy of the tower will be equal to:

$$T_t(t) = \frac{1}{2} M_{ty} \dot{v}(r, t)^2 |_{r=r_0} \quad (2.39)$$

The strain energy of the tower will be equal to:

$$U_t(t) = \frac{1}{2} K_v v(r_0, t)^2 \quad (2.40)$$

Afterwards the kinetic energy and the strain energy of the tower will be added correspondingly to the kinetic and strain energy of the blade which are defined in equations 2.16 and 2.10.

The tower will influence the equations of motion only at the boundary of the flapwise direction at the point where the blade connects to the tower. As a result after using Hamilton's principle the resultant boundaries will be:

At $r = r_0$

$$\frac{\partial v(r, t)}{\partial r} |_{r=r_0} = 0$$

$$(EI_{yy}v'''(r, t) + EI_{xy}u'''(r, t))|_{r=r_0} = \{Tn(r)(v(r, t) + \cos(\beta(r))\phi(r, t)e(r) + \sin(\beta(r))e(r))'\}|_{r=r_0} - K_v v(r_0, t) - M_{ty} \ddot{v}(r, t) |_{r=r_0} \quad (2.41)$$

The first equation represents the slope of the blade which will be zero at the point where it connects to the blade and the second one represents the shear force which includes also the force due to the stiffness of the spring and the force due to the existence of the mass.

3

Finite Element Analysis

In this specific chapter the finite element analysis of the blade will be illustrated. The finite element method is a numerical method that can be used for an accurate (but approximate) solution of many complex vibration problems. The mass and stiffness matrices and force vectors needed for the finite element analysis are derived for the basic one-dimensional elements such as a beam under bending which applies to the case studied. It is really important to note that the finite element method is employed to solve very complex mathematical models, but it is important to realize that the finite element solution can never give more information than that contained in the mathematical model [15]. The approach that finite elements follow is that the engineering problem is simulated as a mathematical model. The model is then solved by discretizing it into numerous finite elements. These finite elements are composed of nodes which interconnect all the elements and they are also used to define the degrees of freedom (DOF) of the element. These nodes are generally located at the edges of the finite element and in order to obtain the solution within the element, approximate interpolation functions (also known as shape functions or basis functions) are used. However, in reality, engineering problems consist of an infinite number of elements with an infinite number of DOF, which is not efficient to be solved using the FEM and thus, the term approximate is referred. The mathematical model is basically a set of partial differential equations. In this case, it is represented by the partial differential equations of motion, along with the sets of boundary conditions, derived in the preceding chapter. However, few details that are required for this project are represented in the following sections.

3.1. Beam Element

As mentioned before the finite element analysis includes discretization of the model into finite element. In this specific case, as the blade has characteristics of a beam, it will be modeled by beam elements. The discussed degrees of freedom of the blade are flapwise bending (\tilde{y} -direction), edgewise bending (\tilde{z} -direction) and torsion.

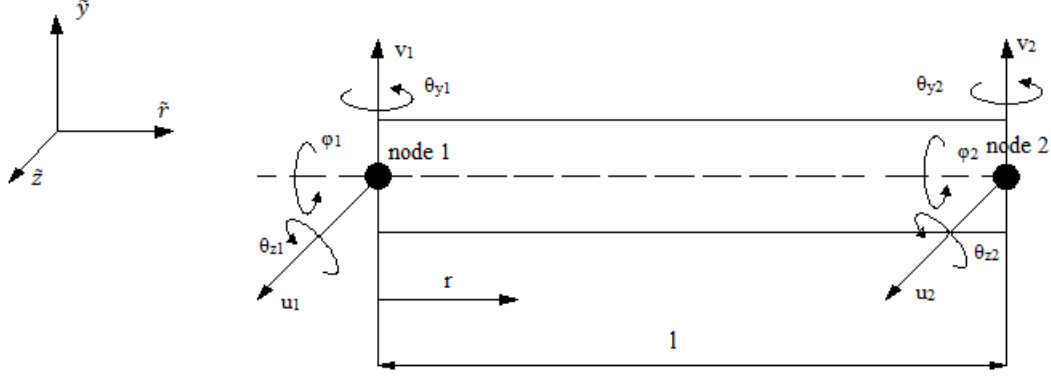


Figure 3.1: Degrees of freedom applied to a beam element

As it is obvious from the above figure each element consists of two nodes and the degrees of freedom applied to each element's node are five :

- u_1 : transverse deflection in \tilde{z} -direction
- θ_{z1} : bending around \tilde{z} -axis
- v_1 : transverse deflection in \tilde{y} -direction
- θ_{y1} : bending around \tilde{y} -axis
- ϕ_1 torsion around \tilde{r} - axis

3.2. Discretization of the Blade

As mentioned before in order to model the blade using finite element analysis it should be first discretized. In order to achieve this the appropriate interpolation function should be used as it assures inter- element continuity of the nodal DOF. Since in the beam element model defined previously the bending slopes are taken into consideration the interpolation function used for bending deflection in \tilde{r} , \tilde{z} plane will be:

$$u = a_0 + a_1 r + a_2 r^2 + a_3 r^3 \quad (3.1)$$

The coefficients a_0 , a_1 , a_2 , a_3 are obtained using the boundary conditions of the beam element and it is elaborated in [16] and [15]. The same formulation as above can be adopted for the \tilde{y} , \tilde{r} plane. As a result the final expressions for the per element bending deflections are:

$$u_e(r, t) = N_1(r)u_1(t) + N_2(r)\theta_{x1}(t) + N_3(r)u_2(t) + N_4(r)\theta_{x2}(t) = \mathbf{N}^e(r)\mathbf{u}^e(t) \quad (3.2)$$

$$v_e(r, t) = N_1(r)v_1(t) + N_2(r)\theta_{y1}(t) + N_3(r)v_2(t) + N_4(r)\theta_{y2}(t) = \mathbf{N}^e(r)\mathbf{v}^e(t) \quad (3.3)$$

Where $N_1(r)$, $N_2(r)$, $N_3(r)$, $N_4(r)$ are the shape functions equal to:

$$N_1(r) = 1 - 3\left(\frac{r}{l}\right)^2 + 2\left(\frac{r}{l}\right)^3 \quad (3.4)$$

$$N_2(r) = r - 2l\left(\frac{r}{l}\right)^2 + l\left(\frac{r}{l}\right)^3 \quad (3.5)$$

$$N_3(r) = 3\left(\frac{r}{l}\right)^2 - 2\left(\frac{r}{l}\right)^3 \quad (3.6)$$

$$N_4(r) = -l\left(\frac{r}{l}\right)^2 + l\left(\frac{r}{l}\right)^3 \quad (3.7)$$

As far as the torsion is concerned, the equations for discretization are:

$$\phi_e(r, t) = N_1^*(r)\phi_1(t) + N_2^*(r)\phi_2(t) = \mathbf{N}^{*e}(r)\boldsymbol{\phi}^e(t) \quad (3.8)$$

Where the shape functions are equal to :

$$N_1^*(r) = \left(1 - \frac{r}{l}\right) \quad (3.9)$$

$$N_2^*(r) = \frac{r}{l} \quad (3.10)$$

Having formulated the per element distribution of the blade deformations, the subsequent steps involve the derivation of the element mass and stiffness matrices, and assembling them to the corresponding global matrices. These steps are elaborated in the following section.

3.3. Stiffness and Mass Matrices

The stiffness and mass matrices are obtained after substituting equations 3.2, 3.37 and 3.8 into the equations of kinetic and strain energy and then integrating over the length of the element l . Afterwards, Hamilton's principle is applied in order to obtain the discretized form of the equations for the different directions.

In order to simplify the equations of motion some notations have been introduced which are represented below. In the subsequent expressions, the annotations ()_e and ()^T have been used to represent the per element characteristics of the terms and matrix transpose operation, respectively.

$$\mathbf{M} = \int_0^l \mathbf{N}^e(r)^T \mathbf{N}^e(r) m^e dr \quad (3.11a)$$

$$\mathbf{M}_T^* = \int_0^l \mathbf{N}^e(r)^T \mathbf{N}^{*e}(r) m^e dr \quad (3.11b)$$

$$\mathbf{M}^* = \int_0^l \mathbf{N}^{*e}(r)^T \mathbf{N}^{*e}(r) m^e dr \quad (3.11c)$$

$$\mathbf{J} = \int_0^l \mathbf{N}^{*e}(r)^T \mathbf{N}^{*e}(r) J^e dr \quad (3.11d)$$

$$\mathbf{K}_{B;xx}^e = \int_0^l \mathbf{N}^{e''}(r)^T \mathbf{N}^{e''}(r) EI_{xx}^e dr \quad (3.11e)$$

$$\mathbf{K}_{B;yy}^e = \int_0^l \mathbf{N}^{e''}(r)^T \mathbf{N}^{e''}(r) EI_{yy}^e dr \quad (3.11f)$$

$$\mathbf{K}_{B;xy}^e = \int_0^l \mathbf{N}^{e''}(r)^T \mathbf{N}^{e''}(r) EI_{xy}^e dr \quad (3.11g)$$

$$\mathbf{K}_{T;zz}^e = \int_0^l \mathbf{N}^{*e'}(r)^T \mathbf{N}^{*e'}(r) GJ^e dr \quad (3.11h)$$

$$\mathbf{K}_c^e = \int_0^l \mathbf{N}^{e'}(r)^T \mathbf{N}^{e'}(r) p^e dr \quad (3.11i)$$

$$\mathbf{K}_{c;T}^{*e} = \int_0^l \mathbf{N}^{*e'}(r)^T \mathbf{N}^{*e'}(r) p^e dr \quad (3.11j)$$

$$\mathbf{K}_c^{*e} = \int_0^l \mathbf{N}^{*e'}(r)^T \mathbf{N}^{*e'}(r) p^e dr \quad (3.11k)$$

$$\mathbf{F}^e = \int_0^l \mathbf{N}^e(r)^T m^e dr \quad (3.11l)$$

$$\mathbf{F}^{*e} = \int_0^l \mathbf{N}^{*e}(r)^T m^e dr \quad (3.11m)$$

After substituting the above equations into the kinetic and strain energy, the discretized form of them is:

Strain Energy

$$\begin{aligned} \mathbf{U}^e(t) = & \frac{1}{2} \mathbf{u}^e(t)^T \mathbf{K}_{B;xx}^e \mathbf{u}^e(t) + \frac{1}{2} \mathbf{v}^e(t)^T \mathbf{K}_{B;yy}^e \mathbf{v}^e(t) + \frac{1}{2} \boldsymbol{\varphi}^e(t)^T \mathbf{K}_{T;zz}^e \boldsymbol{\varphi}^e(t) + \\ & \mathbf{u}^e(t)^T \mathbf{K}_{B;xy}^e \mathbf{v}^e(t) + \frac{1}{2} \mathbf{u}^e(t)^T \mathbf{K}_c^e \mathbf{u}^e(t) + \frac{1}{2} \mathbf{v}^e(t)^T \mathbf{K}_c^e \mathbf{v}^e(t) + \\ & \frac{1}{2} \boldsymbol{\varphi}^e(t)^T \mathbf{K}_c^{*e} \boldsymbol{\varphi}^e(t) e^2 - \mathbf{u}^e(t)^T \mathbf{K}_{c;T}^{*e} \boldsymbol{\varphi}^e(t) e \sin(\beta) \\ & + \mathbf{v}^e(t)^T \mathbf{K}_{c;T}^{*e} \boldsymbol{\varphi}^e(t) e \cos(\beta) + \mathbf{u}^e(t)^T \mathbf{F}^e g \sin(\psi(t)) - \\ & \boldsymbol{\varphi}^e(t)^T \mathbf{F}^{*e} g e \sin(\psi(t)) \sin(\beta) \end{aligned} \quad (3.12)$$

Kinetic Energy

$$\begin{aligned} \mathbf{T}^e(t) = & \frac{1}{2} \dot{\mathbf{u}}^e(t)^T \mathbf{M} \dot{\mathbf{u}}^e(t) + \frac{1}{2} \dot{\mathbf{v}}^e(t)^T \mathbf{M} \dot{\mathbf{v}}^e(t) + \frac{1}{2} \dot{\boldsymbol{\varphi}}^e(t)^T \mathbf{J} \dot{\boldsymbol{\varphi}}^e(t) \\ & + \frac{1}{2} \mathbf{u}^e(t)^T \mathbf{M} \mathbf{u}^e(t) \Omega^2 - \mathbf{u}^e(t)^T \mathbf{M}_T^* \boldsymbol{\varphi}^e(t) \Omega^2 e \sin(\beta) \\ & + \frac{1}{2} \boldsymbol{\varphi}^e(t)^T \mathbf{M}^* \boldsymbol{\varphi}^e(t) \Omega^2 e^2 \sin(\beta)^2 + \frac{1}{2} \dot{\boldsymbol{\varphi}}^e(t)^T \mathbf{M}^* \dot{\boldsymbol{\varphi}}^e(t) e^2 \\ & + \dot{\mathbf{v}}^e(t)^T \mathbf{M}_T^* \boldsymbol{\varphi}^e(t) e \cos(\beta) - \dot{\mathbf{u}}^e(t)^T \mathbf{M}_T^* \dot{\boldsymbol{\varphi}}^e(t) e \sin(\beta) \\ & + \mathbf{u}^e(t)^T \mathbf{F}^e e \Omega^2 \cos(\beta) - \boldsymbol{\varphi}^e(t)^T \mathbf{F}^{*e} e^2 \Omega^2 \sin(\beta) \cos(\beta) \end{aligned} \quad (3.13)$$

It should be noted that in the above expressions, a discrete value (averaged) for the eccentricity of the center of mass (COM) and the pre-twist angle (β) are assigned per element. This has been done in order to simplify the equations.

Formulation of discretized equations of motion

The Lagrangian function per element is defined as follows:

$$\mathbf{L}^e(t) = \mathbf{T}^e(t) - \mathbf{U}^e(t) \quad (3.14)$$

The equations of motion are derived by using Hamilton's Principle as defined in equation 2.20. However the principle is redefined since the displacements depend now only on time. As a result the expression used is illustrated below.

$$\frac{\partial \mathbf{L}^e(t)}{\partial \mathbf{u}_b^e(t)} - \frac{\partial}{\partial t} \frac{\partial \mathbf{L}^e(t)}{\partial \dot{\mathbf{u}}_b^e} = 0 \quad (3.15)$$

Using the equations 3.14 and 3.15 the discretized equations of motion can be expressed as:

$$\mathbf{M}^e \ddot{\mathbf{u}}_b^e(t) + \mathbf{K}^e \mathbf{u}_b^e(t) = \mathbf{F}^e(t) \quad (3.16)$$

Where \mathbf{M}^e , \mathbf{K}^e and \mathbf{F}^e are the element mass, stiffness and force matrices, respectively. These matrices can be elaborated as follows:

$$\mathbf{M}^e = \begin{bmatrix} \mathbf{J} + \mathbf{M}^* e^2 & (\mathbf{M}_T^*)^T e \cos(\beta) & (\mathbf{M}_T^*)^T e \sin(\beta) \\ \mathbf{M}_T^* e \cos(\beta) & \mathbf{M} & \mathbf{0} \\ \mathbf{M}_T^* e \sin(\beta) & \mathbf{0} & \mathbf{M} \end{bmatrix} \quad (3.17)$$

$$\mathbf{K}^e = \mathbf{K}_B^e + \mathbf{K}_T^e - \mathbf{K}_G^e \quad (3.18)$$

Where:

$$\mathbf{K}_B^e = \begin{bmatrix} \mathbf{K}_{T;zz}^e & \mathbf{0}_{2 \times 4} & \mathbf{0}_{2 \times 4} \\ \mathbf{0}_{4 \times 2} & \mathbf{K}_{B;yy}^e & \mathbf{K}_{B;xy}^e \\ \mathbf{0}_{4 \times 2} & \mathbf{K}_{B;xy}^e & \mathbf{K}_{B;xx}^e \end{bmatrix} \quad (3.19)$$

$$\mathbf{K}_T^e = \begin{bmatrix} \mathbf{K}_C^{*e} e^2 & (\mathbf{K}_{C;T}^{*e})^T e \cos(\beta) & -(\mathbf{K}_{C;T}^{*e})^T e \sin(\beta) \\ \mathbf{K}_{C;T}^{*e} e \cos(\beta) & \mathbf{K}_C^e & \mathbf{0}_{4 \times 4} \\ -\mathbf{K}_{C;T}^{*e} e \sin(\beta) & \mathbf{0}_{4 \times 4} & \mathbf{K}_C^e \end{bmatrix} \quad (3.20)$$

$$\mathbf{K}_G^e = \begin{bmatrix} \mathbf{M}^* \sin^2(\beta) e^2 \Omega^2 & \mathbf{0}_{2 \times 4} & -(\mathbf{M}_T^*)^T e \sin(\beta) \Omega^2 \\ \mathbf{0}_{4 \times 2} & \mathbf{0}_{4 \times 4} & \mathbf{0}_{4 \times 4} \\ -(\mathbf{M}_T^*)^T e \sin(\beta) \Omega^2 & \mathbf{0}_{4 \times 4} & \Omega^2 \mathbf{M} \end{bmatrix} \quad (3.21)$$

The expressions of the submatrices \mathbf{M} , \mathbf{J} , \mathbf{M}^* , $\mathbf{K}_{B;xx}^e$, $\mathbf{K}_{B;xy}^e$, $\mathbf{K}_{B;yy}^e$, $\mathbf{K}_{T;zz}^e$ and \mathbf{K}_C^e in the element mass and stiffness matrices can be found in the literature [15], [16] and [17].

The matrix \mathbf{M}_T^* which is used to express the coupling between bending and torsion is elaborated as follows:

$$\mathbf{M}_T^* = m_e \begin{bmatrix} \frac{7l}{20} & \frac{3l}{20} \\ \frac{l^2}{20} & \frac{l^2}{30} \\ \frac{3l}{20} & \frac{7l}{20} \\ \frac{l^2}{-30} & \frac{l^2}{-20} \end{bmatrix} \quad (3.22)$$

The centrifugal stiffness submatrix associated to the torsion is decomposed into three matrices which are expressed as:

$$\mathbf{K}_C^{*e} = \mathbf{K}_{C;1}^{*e} + \mathbf{K}_{C;2}^{*e} + \mathbf{K}_{C;3}^{*e} \quad (3.23)$$

Where:

$$\mathbf{K}_{C;1}^{*e} = p_1^e \begin{bmatrix} \frac{1}{l} & \frac{-1}{l} \\ \frac{-1}{l} & \frac{1}{l} \end{bmatrix} \quad (3.24)$$

$$\mathbf{K}_{C;2}^{*e} = p_2^e \begin{bmatrix} \frac{1}{2} & \frac{-1}{2} \\ \frac{-1}{2} & \frac{1}{2} \end{bmatrix} \quad (3.25)$$

$$\mathbf{K}_{C;3}^{*e} = p_3^e \begin{bmatrix} \frac{l}{3} & \frac{-l}{3} \\ \frac{-l}{3} & \frac{l}{3} \end{bmatrix} \quad (3.26)$$

In the same manner the submatrices which correspond to the coupling terms in the centrifugal stiffness matrix are further decomposed into three matrices which are illustrated below:

$$\mathbf{K}_{C;T}^{*e} = \mathbf{K}_{C;T1}^{*e} + \mathbf{K}_{C;T2}^{*e} + \mathbf{K}_{C;T3}^{*e} \quad (3.27)$$

$$\mathbf{K}_{C;T1}^{*e} = p_1^e \begin{bmatrix} \frac{l}{l} & \frac{-l}{l} \\ 0 & 0 \\ \frac{-l}{l} & \frac{l}{l} \\ 0 & 0 \end{bmatrix} \quad (3.28)$$

$$\mathbf{K}_{C;T2}^{*e} = p_2^e \begin{bmatrix} \frac{1}{2} & \frac{-1}{2} \\ \frac{l}{12} & \frac{-l}{12} \\ \frac{-1}{2} & \frac{1}{2} \\ \frac{l}{12} & \frac{l}{12} \end{bmatrix} \quad (3.29)$$

$$\mathbf{K}_{C;T3}^{*e} = p_3^e \begin{bmatrix} \frac{3l}{10} & \frac{-3l}{10} \\ \frac{l^2}{15} & \frac{-l^2}{15} \\ \frac{-3l}{10} & \frac{3l}{10} \\ \frac{l^2}{10} & \frac{l^2}{10} \end{bmatrix} \quad (3.30)$$

In all the above expressions the term p^e represents the axial force acting on the blade. Similarly to the submatrices this is split into three parts p_1^e , p_2^e and p_3^e . The reason being due to the dependency of 'Pe' on the radial distance r which gets involved [18] in the integration procedure. In addition for this specific project the effect of gravity is introduced.

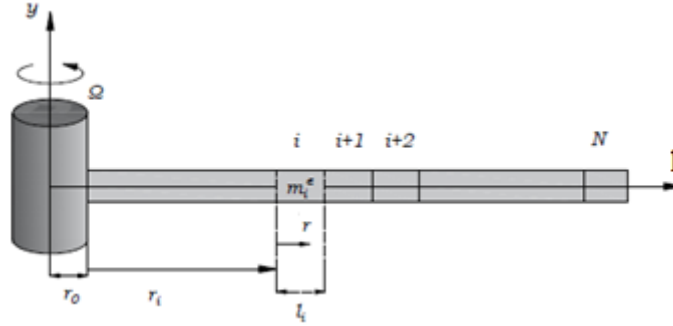


Figure 3.2: Discretization of the Blade

The three components of the centrifugal force for the i^{th} element will be equal to :

$$p_1^e = \Omega^2 m_i^e \{(r_0 + r_i)l_i + l_i^2\} - g \cos(\psi)l_i$$

$$+ \Omega^2 \sum_{n=1}^N m_{n+1}^e \{r_0(r_{n+2} - r_{n+1}) + \frac{1}{2}(r_{n+2}^2 - r_{n+1}^2) - g \cos(\psi)(r_{n+2} - r_{n+1})\} \quad (3.31)$$

$$p_2^e = -m_i^e \{\Omega^2(r_0 + r_i) - g \cos(\psi)\} \quad (3.32)$$

$$p_3^e = -\frac{1}{2}m_i^e \Omega^2 \quad (3.33)$$

The force submatrices, \mathbf{F}^e and \mathbf{F}^{*e} can be elaborated as follows:

$$\mathbf{F}^e = m^e \begin{bmatrix} \frac{l}{2} \\ \frac{l^2}{12} \\ \frac{l}{2} \\ -\frac{l}{12} \end{bmatrix} \quad (3.34)$$

$$\mathbf{F}^{*e} = m^e \begin{bmatrix} \frac{l}{2} \\ \frac{l}{2} \end{bmatrix} \quad (3.35)$$

3.4. Assembling the Global Matrices

In order to be able to solve later the finite element model the element and stiffness matrices should be assembled in the corresponding global matrices. This is achieved by locating the values of the element nodal DOF in order to obtain the global configuration of the nodal DOF and then lump them into global matrices.

The element mass and stiffness matrices have initially the local configuration which is illustrated below.

$$A_{local} = \begin{matrix} & \begin{matrix} u_1 & \theta_{x1} & u_2 & \theta_{x2} & v_1 & \theta_{y1} & v_2 & \theta_{y2} & \phi_1 & \phi_2 \end{matrix} \\ \begin{matrix} u_1 \\ \theta_{x1} \\ u_2 \\ \theta_{x2} \\ v_1 \\ \theta_{y1} \\ v_2 \\ \theta_{y2} \\ \phi_1 \\ \phi_2 \end{matrix} & \begin{pmatrix} a_{1,1} & a_{1,2} & \cdots & \cdots & \cdots & \cdots & \cdots & \cdots & a_{1,9} & a_{1,10} \\ a_{2,1} & a_{2,2} & \cdots & \cdots & \cdots & \cdots & \cdots & \cdots & a_{2,9} & a_{2,10} \\ \vdots & \vdots & \ddots & & & & & & \vdots & \vdots \\ \vdots & \vdots & & \ddots & & & & & \vdots & \vdots \\ \vdots & \vdots & & & \ddots & & & & \vdots & \vdots \\ \vdots & \vdots & & & & \ddots & & & \vdots & \vdots \\ \vdots & \vdots & & & & & \ddots & & \vdots & \vdots \\ \vdots & \vdots & & & & & & \ddots & \vdots & \vdots \\ a_{1,9} & a_{2,9} & \cdots & \cdots & \cdots & \cdots & \cdots & \cdots & a_{9,9} & a_{9,10} \\ a_{1,10} & a_{2,10} & \cdots & \cdots & \cdots & \cdots & \cdots & \cdots & a_{9,10} & a_{10,10} \end{pmatrix} \end{matrix}$$

Figure 3.3: Local Configuration of the nodal DOFs

The values in this matrix are then re-arranged to fit into the corresponding nodal DOF in the global configuration. The new configuration of the nodal DOFs will be :

$$A_{global} = \begin{matrix} & \begin{matrix} u_1 & \theta_{x1} & v_1 & \theta_{y1} & \phi_1 & u_2 & \theta_{x2} & v_2 & \theta_{y2} & \phi_2 \end{matrix} \\ \begin{matrix} u_1 \\ \theta_{x1} \\ v_1 \\ \theta_{y1} \\ \phi_1 \\ u_2 \\ \theta_{x2} \\ v_2 \\ \theta_{y2} \\ \phi_2 \end{matrix} & \begin{pmatrix} a_{1,1} & a_{1,2} & \cdots & \cdots & \cdots & \cdots & \cdots & \cdots & a_{1,8} & a_{1,10} \\ a_{2,1} & a_{2,2} & \cdots & \cdots & \cdots & \cdots & \cdots & \cdots & a_{2,8} & a_{2,10} \\ \vdots & \vdots & \ddots & & & & & & \vdots & \vdots \\ \vdots & \vdots & & \ddots & & & & & \vdots & \vdots \\ \vdots & \vdots & & & \ddots & & & & \vdots & \vdots \\ \vdots & \vdots & & & & \ddots & & & \vdots & \vdots \\ \vdots & \vdots & & & & & \ddots & & \vdots & \vdots \\ \vdots & \vdots & & & & & & \ddots & \vdots & \vdots \\ a_{1,8} & a_{2,8} & \cdots & \cdots & \cdots & \cdots & \cdots & \cdots & a_{8,8} & a_{8,10} \\ a_{1,10} & a_{2,10} & \cdots & \cdots & \cdots & \cdots & \cdots & \cdots & a_{8,10} & a_{10,10} \end{pmatrix} \end{matrix}$$

Figure 3.4: Global Configuration of the nodal DOFs

Note that the mass and stiffness matrices defined in both the local and global configurations are symmetric about their diagonal terms. The globally configured element matrices are then assembled into the global matrices as demonstrated

3.6. Introduction of the Tower

In order to add the tower into the finite element analysis the mass matrix and the stiffness matrix of the beam element will be transformed.

According to literature [16] the mass matrix of the beam element is equal to:

$$\mathbf{M} = m^e \begin{bmatrix} \frac{156l}{420} & \frac{22l^2}{420} & \frac{54l}{420} & \frac{-13l^2}{420} \\ \frac{22l^2}{420} & \frac{4l^3}{420} & \frac{13l^2}{420} & \frac{-3l^3}{420} \\ \frac{54l}{420} & \frac{13l^2}{420} & \frac{156l}{420} & \frac{-22l^2}{420} \\ \frac{-13l^2}{420} & \frac{-3l^3}{420} & \frac{-22l^2}{420} & \frac{4l^3}{420} \end{bmatrix} \quad (3.36)$$

and the expression for the per element bending deflection according to equation 3.37 at $\tilde{r}=0$ will be equal to:

$$v_e(r, t) = v_1(t) \quad (3.37)$$

As a result the mass of the tower will be added to the mass matrix of the beam element at the cell which corresponds to $v_1(t)$. the resultant mass matrix for the beam element as flapwise deformation only is concerned will be as follows:

$$\mathbf{M} = m^e \begin{bmatrix} \frac{156l}{420} + M_{ty} & \frac{22l^2}{420} & \frac{54l}{420} & \frac{-13l^2}{420} \\ \frac{22l^2}{420} & \frac{4l^3}{420} & \frac{13l^2}{420} & \frac{-3l^3}{420} \\ \frac{54l}{420} & \frac{13l^2}{420} & \frac{156l}{420} & \frac{-22l^2}{420} \\ \frac{-13l^2}{420} & \frac{-3l^3}{420} & \frac{-22l^2}{420} & \frac{4l^3}{420} \end{bmatrix} \quad (3.38)$$

Correspondingly the new stiffness matrix will be equal to :

$$\mathbf{K} = \frac{EI_{yy}}{l^3} \begin{bmatrix} 12 + K_v & 6l & -12 & 6l \\ 6l & 4l^2 & -6l & 2l^2 \\ -12 & -6l & 12 & -6l \\ 6l & 2l^2 & -6l & 4l^2 \end{bmatrix} \quad (3.39)$$

In order to represent the tower as realistic as possible the first natural fore- aft frequency of the tower will be used according to literature [8] in order to calibrate the values of mass and the stiffness of the tower, which will be introduced into the finite element model.

Initially the stiffness of the tower was calculated using the formula of static stiffness.

$$K = \frac{3EI}{l^3} = 966914.5333N/m \quad (3.40)$$

In the above equation the Young's Modulus according to [8] was considered equal to 210 GPa . The second moment of area of the tower [21] can be obtained from the following formula .

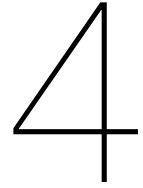
$$I = \frac{\pi}{64}(D^4 - (D - 2t_h)^4) \quad (3.41)$$

In which D is the tower mean external diameter which is equal to 4.875 m and the tower shell thickness is equal to 0.023m.

Using this specific stiffness into the finite element model after calibration the first fore-aft natural frequency of the tower was achieved by utilizing a mass equal to 215800 kg. This quantity is equal to 62.1% of the mass of the tower. According to literature [24] the first effective modal mass for a cantilever beam is equal to:

$$m_{eff,1} = 0.6139 * m_{tower} \quad (3.42)$$

Which is obviously really close to the actual value of mass used in the model.



Eigenanalysis

The purpose of eigenanalysis is to determine the eigenvalues and eigenmodes of a vibrating system under zero external force. The term eigenvalues is correlated to the natural frequencies of the system and the term eigenmodes is correlated to the response of the system to that free vibration. The acknowledgment of the natural frequencies is really important since resonance phenomena can be avoided. For instance, during the design of a structure which might undergo an earthquake in the future, by knowing the most probable case scenario of earthquake in the area (spectrum, magnitude, etc) and the natural frequencies of the structure a more secure structural design of the structure can be achieved.

In order to perform the eigenanalysis the force matrices will not be introduced in the finite element model, which will result in the free vibration problem. As a result only the mass and stiffness matrices will be utilized for the eigenanalysis. The eigenvalue problem is stated as follows:

$$\{\mathbf{K} - \omega^2 \mathbf{M}\}u = 0 \quad (4.1)$$

Afterwards the boundary conditions should be introduced to the model leading to 'n' number of quantities which are the eigenvalues (ω^2) and its quantity has a corresponding modal amplitude vector which is the eigenmode (u). The square root of the eigenvalues result in the natural frequencies of the system. In the specific case studied since the blade is discretized into finite elements, the number of natural frequencies and eigenmodes will be equal to the number of finite elements used during the solution of the model.

4.1. Eigenvalues and Eigenmodes

The eigenvalues and eigenmodes of the model will be determined using the numerical computation software Matlab and more specifically some inbuilt functions of it. In the following sections the coupled model of the blade will be illustrated for the coordinate frame defined in the preceding chapters and afterwards the model of the blade including the tower will be illustrated.

4.1.1. Coupled bending twist vibration

Initially the eigenmodes of the blade for the coupled case will be generated. The structural properties of the blade are based on the NREL 5 MW manual [8]. The length of the blade from the hub axis is 63 m and the radius of the hub is 1.5m. The geometry of the blade is described by its radially varying pre-twist and the chord length. The natural frequencies generated are listed in Table 4.1. It should be noted that these frequency values are derived for the blade in a standstill state, that is non-rotating, with the blade azimuth as '0 rad'.

Table 4.1: Coupled Model

Natural Frequencies (Hz)		
Mode	Mode Type	Coupled Model
1	Flapwise	0.692
2	Edgewise	1.110
3	Flapwise	1.996
4	Edgewise	4.096
5	Flapwise	4.622
6	Torsion	5.590

4.1.2. Coupled vibration of a standstill and a rotating blade

In this section the influence of rotation and gravity on the dynamic response of the blade are studied. According to literature [8] the rated wind speed of the 5MW wind turbine is 11.4 m/s and its corresponding rotor speed is 12.1 rpm. The first six natural frequencies for this data are represented on Table 4.2.

Table 4.2: Standstill versus rotating blade

Natural Frequencies (Hz)				
Mode	Standstill Model with $g = 0m/s^2$	Rotating model with $g = 0m/s^2$	Rotating model with g and $a = 0^\circ$	Rotating model with g and $a = \pi^\circ$
1	0.692	0.744	0.737	0.750
2	1.110	1.154	1.150	1.157
3	1.996	2.055	2.048	2.061
4	4.096	4.127	4.124	4.131
5	4.622	4.674	4.668	4.681
6	5.590	5.592	5.592	5.592

It can be seen from the results that when rotation is added to the model the natural frequencies of the blade are increased which means that the structure becomes more stiff. This can be interpreted as stiffening effect induced by the centrifugal force applied to the blade. In addition to the above it is obvious that depending on the blade azimuth angle the effect of gravity differs. The maximum frequencies appear for blade azimuth angle equal to π radians and the minimum (with gravity) appear for 0 radians. This happens due to the fact that gravity induces a periodic loading to the blade. However since the variation is small it can be assumed stationary. In addition to that the analysis was performed using zero pitch angle.

Following the eigenmodes of the blade will be presented for the standstill case. For the rotating case the eigenmodes are found to be similar to that of standstill.

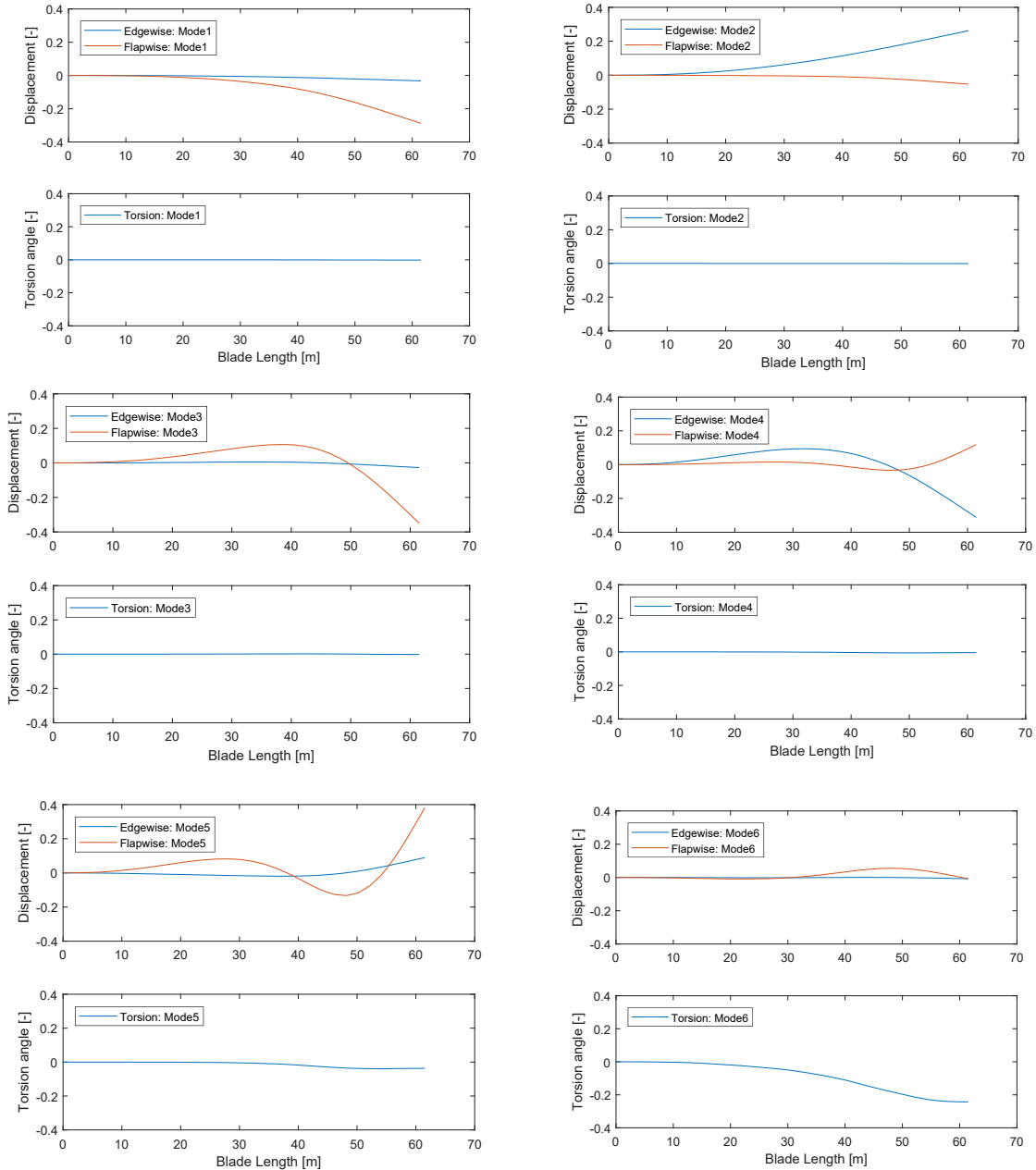


Figure 4.1: Eigenmodes of a standstill Blade

The eigenmodes represented in Figure 4.1 are normalized by their magnitude more specifically:

$$\hat{\mathbf{u}} = \frac{\mathbf{u}}{|\mathbf{u}|} \quad (4.2)$$

Where $\hat{\mathbf{u}}$ is the normalized eigenmode, \mathbf{u} is the unnormalized eigenmode and $|\mathbf{u}|$ is the magnitude of the eigenmode.

As it is obvious from Figure 4.1, the blade starts deflecting on the negative direction which means the even though the coordinate system defined in chapter 2.1 is positive, due to the form of the coordinates utilized, the blade will most probably deflect on the negative direction. This needs to be taken into consideration later on the aerodynamic analysis.

4.1.3. Coupled bending twist vibration of the complete model

At this section the natural frequencies and eigenmodes of the blade with the tower will be presented. The characteristic of the tower have been chosen according to the 5 MW manual [8]. The natural frequencies are represented below.

Table 4.3: natural frequencies of the complete model

Natural Frequencies (Hz)				
Mode	Standstill Model with $g = 0m/s^2$	Rotating model with $g = 0m/s^2$	Rotating model with g and $a = 0^\circ$	Rotating model with g and $a = \pi^\circ$
1	0.324	0.324	0.324	0.324
2	0.701	0.753	0.747	0.759
3	1.110	1.154	1.151	1.158
4	2.011	2.069	2.062	2.076
5	4.096	4.128	4.124	4.131
6	4.639	4.691	4.685	4.698
7	5.591	5.593	5.593	5.593

As it is obvious from the Table 4.3 the natural frequencies behave similarly to the natural frequencies of the blade. In addition to that it is obvious that the first natural fore aft frequency of the tower is obtained according to the 5 MW manual [8].

Table 4.4: natural frequencies of the complete model

Natural Frequencies of the blade versus the complete system (Hz)		
Mode	Blade	Blade with Tower
1	0.692	0.324
2	1.110	0.701
3	1.996	1.110
4	4.096	2.011
5	4.622	4.096
6	5.590	4.639
7	-	5.591

Another interested aspect of the model is the effect of the tower on the blade. As it is obvious from Table 4.4 the natural frequencies of the blade after the inclusion of tower have increased slightly. Logically, it was expected that since an extra degree of freedom was added to the system, the system would be less stiff and thus the natural frequencies would be slightly decreased.

In order to explain this effect a much simpler 2 DOF system was constructed, consisting of 2 masses and 2 springs representing the mass of the blade, the mass of the tower, the stiffness of the blade and the stiffness of the tower as illustrated below.

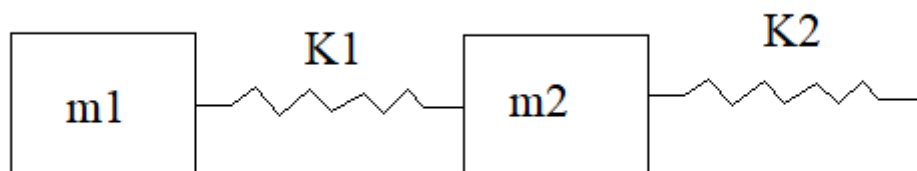


Figure 4.2: Simple 2 DOF system

After solving the above system and increasing the values of K_2 which represents the stiffness of the tower, the natural frequencies fluctuate as follows:

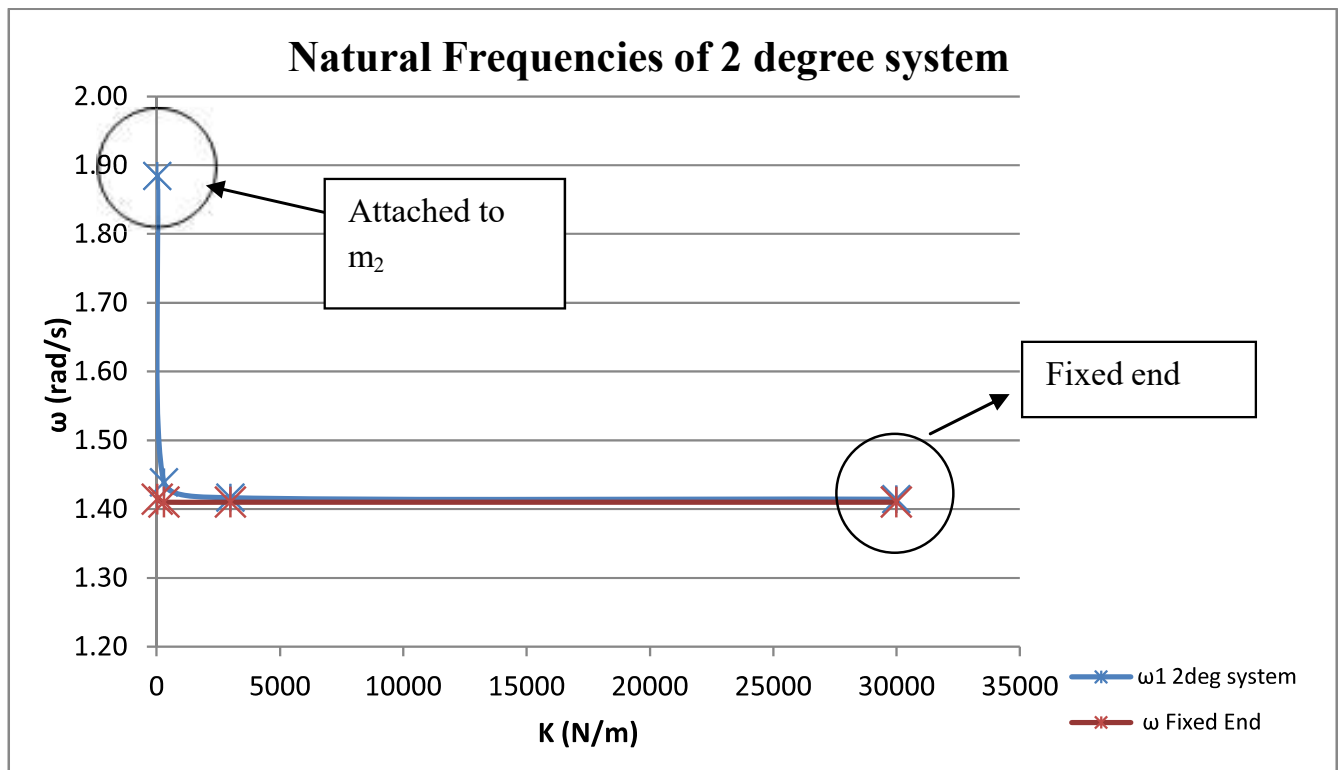


Figure 4.3: Natural Frequencies of 2DOF system

The red line represents the frequencies of the 2 degrees system without m_2 and K_2 (fixed end). The blue line represents the variation of the natural frequency of m_1 (corresponding to the blade). It is obvious that when the stiffness of the spring K_2 increases the natural frequency of the first mass (blade) decreases converging to the value of natural frequency it has with fixed end. This agrees with the behavior of the bending frequencies of the blade as when the tower is added, meaning that the stiffness decreases as from the fixed end situation the blade is attached to the tower, the natural frequencies of the blade increase slightly.

In order to correlate this behavior to the complete model, different values of tower stiffness were utilized and the behavior of the first bending natural frequency of the blade was observed.

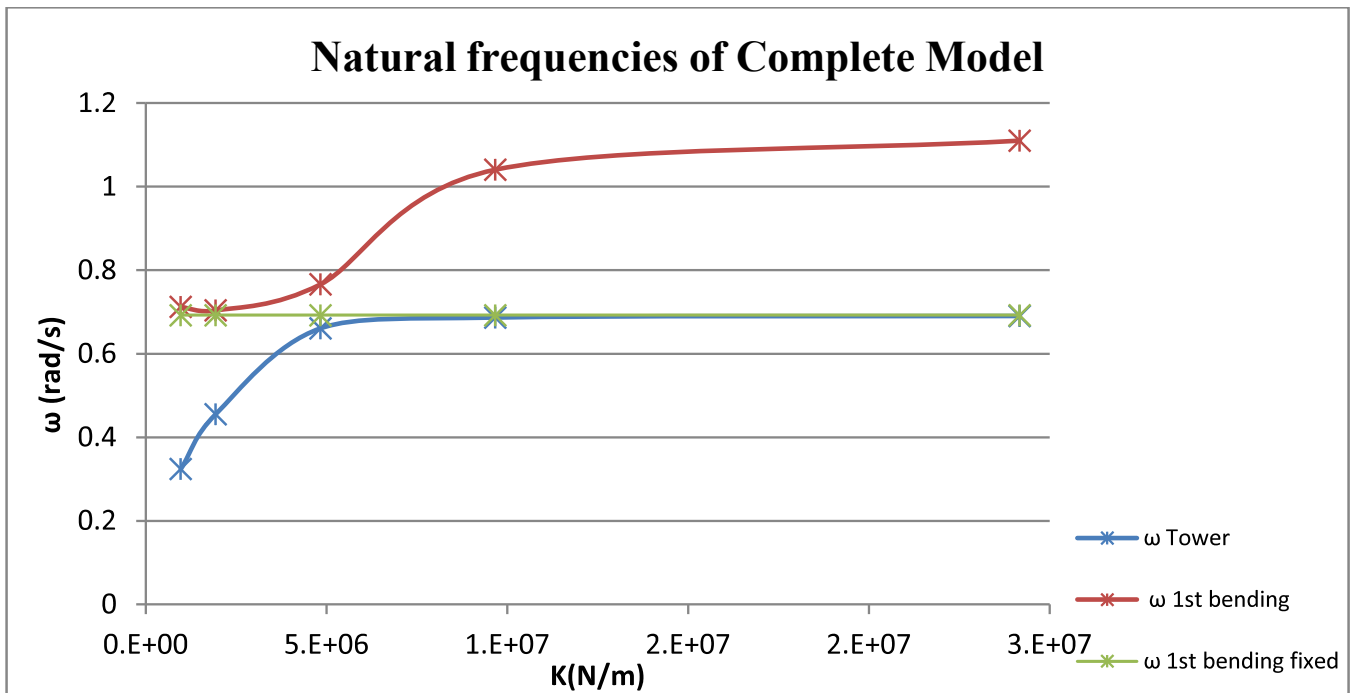


Figure 4.4: Natural Frequencies of complete model

It is obvious that when the stiffness of the tower increases the natural frequency of the tower increases reaching the value of the 1st bending frequency of the blade. Meaning that the tower mode disappears and the system reaches the fixed end situation. Another important observation is that the first bending natural frequency of the blade (red line) while it is slightly increased (first point) it decreases on the second point and after that it increases again reaching the value of the second bending mode of the blade. Generally the behavior of the first bending frequency is similar to the one of m_1 in the 2 DOF system, justifying the increase in the natural frequencies of the blade after the inclusion of the tower.

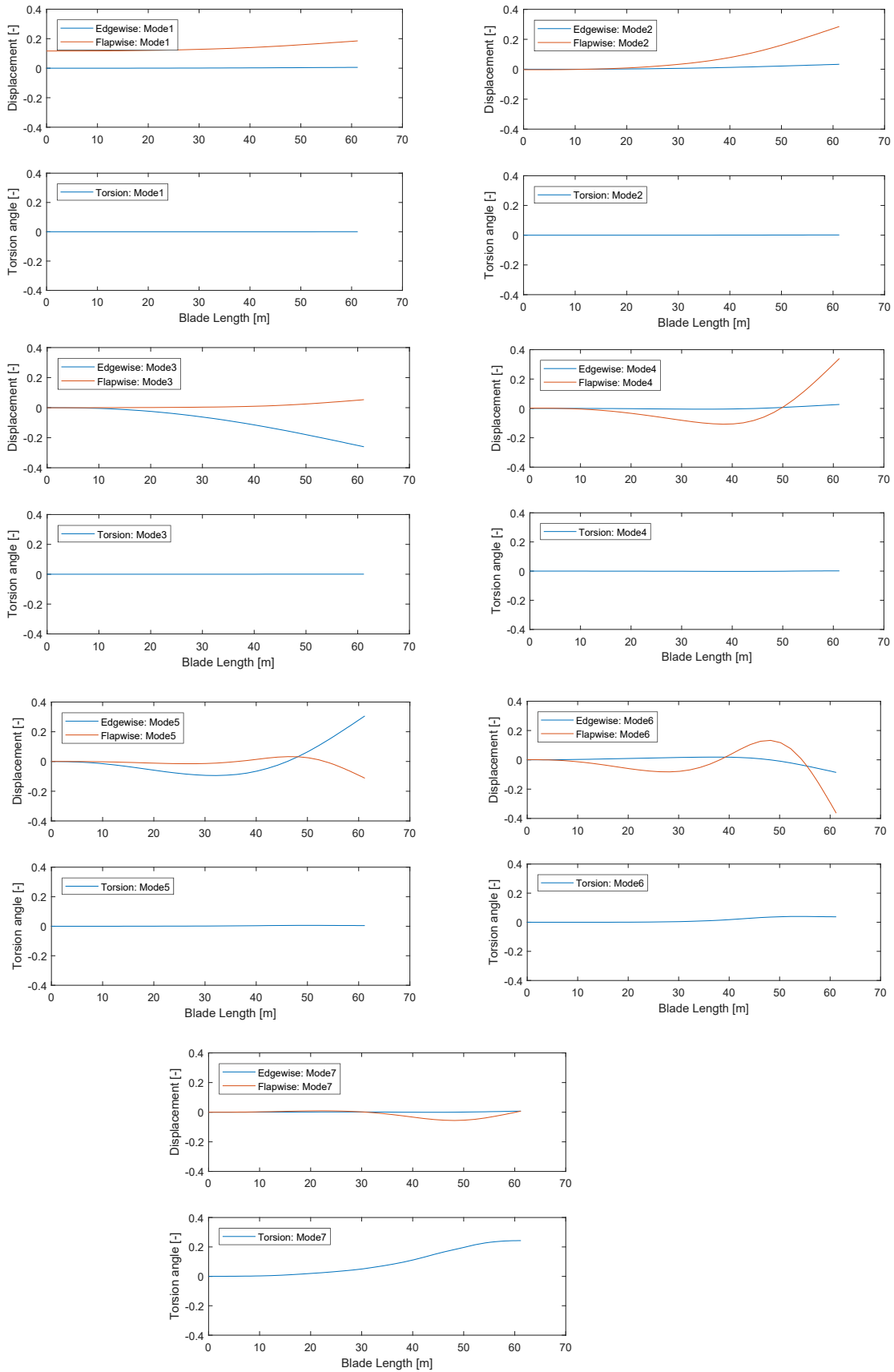


Figure 4.5: Eigenmodes of the complete model

As it is obvious from Figure 4.5 the eigenmodes of the blade with tower are quite different from the eigenmodes of just the blade. First of all, in the first mode there is an initial displacement on the flapwise direction due to the tower and the shape of both flapwise and edgewise eigenmodes is similar to the rigid body mode. It can be observed afterwards that this initial displacement dissipates in the following modes and the blade behaves more like a fixed-end beam. In addition to that the torsional mode is not excited until the seventh mode, similarly to the initial model.

5

Aerodynamic Analysis

The aerodynamic interaction models used in the wind turbine industry come from previous developments in the aircraft industry. The aerodynamic interaction in this particular project is described by instantaneous force models. Such a model neglects the disturbance of the near wake and the consequent delayed development of the new aerodynamic equilibrium. The aerodynamic forcing consists of the lift force and the drag force. In addition to the above forces an additional inertia load is introduced due to the presence of the wind field in which the blade is located. This inertia load can be imitated by a circular cylinder of air, whose diameter is equal to the chord length of the airfoil, which moves with the airfoil [25]. The drag force consists of pressure drag and viscous drag. Pressure drag results from the separation of flow which creates a pressure gradient over the surface of the airfoil and viscous drag is due to the skin friction between the fluid (air) and the surface of the airfoil [3]. In addition to the above another component of drag force, is the induced drag which is induced by wake vorticity. In this particular project attached flow condition is considered thus limiting the drag force to viscous drag alone. Additionally, the flow is assumed to be inviscid and incompressible ($Mach < 0.3$).

The blade of the wind turbine is normally subjected to unsteady aerodynamics, which deals with time-dependent flow velocity, aerodynamic loads, and vortex shedding. For this project, an instantaneous aerodynamic model is assumed for its simplicity. This allows for defining the unsteady aerodynamic loads similar to that of a steady case by considering the characteristics of the system at an instant in time, thus making it a case of quasi-steady aerodynamics .

5.1. Instantaneous Aerodynamic Loading

The loads experienced by the blade under quasi-steady aerodynamics assumption are the following 5.1:

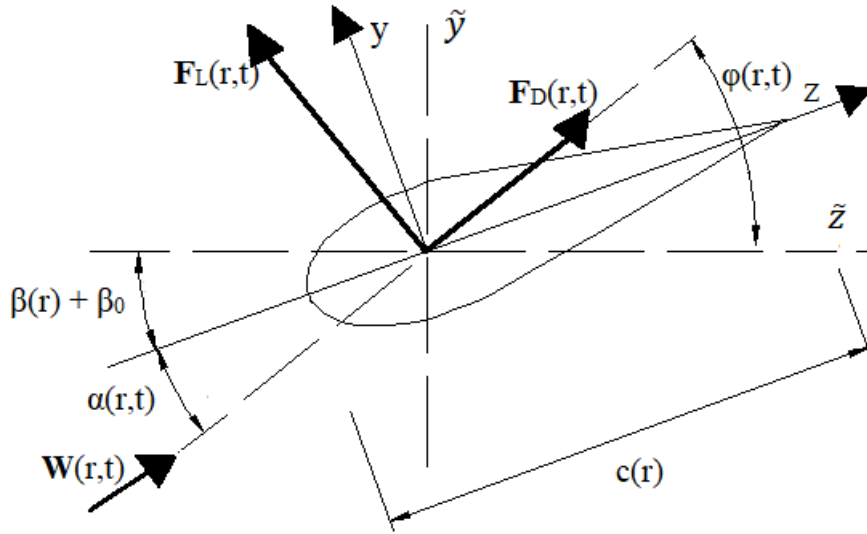


Figure 5.1: Aerodynamic Configuration with the definition of the angle of attack and definition of drag and lift forces

Drag Force

$$\mathbf{F}_D(r, t) = \frac{1}{2} \rho c(r) C_D(r) \mathbf{W}(r, t) |\mathbf{W}(r, t)| \quad (5.1)$$

Lift Force

$$\mathbf{F}_L(r, t) = \rho \mathbf{W}(r, t) \times \mathbf{\Gamma}(r, t) \quad (5.2)$$

Inertia Force

$$\mathbf{F}_I(r, t) = \frac{1}{4} \rho \pi c(r)^2 \dot{\mathbf{W}}(r, t) \quad (5.3)$$

According to [3] the definition of the lift force comes from the Kutta–Joukowski theorem according to which $\mathbf{\Gamma}$ is the circulation of the flow around the airfoil which is generally assumed to be defined at the quarter-chord point from the leading edge.

The circulation of the flow is equal to :

$$\mathbf{\Gamma}(r, t) = \pi c(r) \sin(a(r, t)) |\mathbf{W}(r, t)| \mathbf{e}_r \quad (5.4)$$

where \mathbf{e}_r is the unit vector along the r axis.

In addition the aerodynamic lift coefficient is defined as follows:

$$C_L(r, t) = 2\pi \sin(a(r, t)) \quad (5.5)$$

After substituting equations 5.4 and 5.5 into equation 5.2 the final formula of the lift force is the following:

$$\mathbf{F}_L(r, t) = \frac{1}{2} \rho c(r) C_L(r, t) |\mathbf{W}(r, t)| (\mathbf{W}(r, t) \times \mathbf{e}_r) \quad (5.6)$$

Another really important term used in the above formulas is the relative wind velocity experienced by the blade $\mathbf{W}(r, t)$ which is equal to :

$$\mathbf{W}(r, t) = \mathbf{W}(r) + \mathbf{w}(r, t) - \dot{\mathbf{u}}(r, t) \quad (5.7)$$

where $\mathbf{W}(r)$ is the mean wind velocity, $\mathbf{w}(r, t)$ is the fluctuation of the wind velocity and $\dot{\mathbf{u}}(r, t)$ is the blade vibrational velocity, which includes the aerodynamic interaction. The above velocities are equal to :

$$\mathbf{W}(r) = \begin{bmatrix} 0 \\ W_y(r) \\ \Omega r \end{bmatrix} \quad (5.8)$$

$$\mathbf{w}(r, t) = \begin{bmatrix} 0 \\ w_y(r, t) \\ w_z(r, t) \end{bmatrix} \quad (5.9)$$

$$\dot{\mathbf{u}}(r, t) = \begin{bmatrix} 0 \\ \dot{v}(r, t) + e_{3/4}(r)\cos(\beta(r))\dot{\phi}(r, t) \\ \dot{u}(r, t) - e_{3/4}(r)\sin(\beta(r))\dot{\phi}(r, t) \end{bmatrix} \quad (5.10)$$

After substituting equations 5.8, 5.9 and 5.10 into equation 5.7 the final form of the relative wind velocity is :

$$\mathbf{W}(r, t) = \begin{bmatrix} W_r(r, t) \\ W_y(r, t) \\ W_z(r, t) \end{bmatrix} = \begin{bmatrix} 0 \\ W_y(r) + w_y(r, t) - \dot{v}(r, t) - e_{3/4}(r)\cos(\beta(r))\dot{\phi}(r, t) \\ \Omega r + w_z(r, t) - \dot{u}(r, t) + e_{3/4}(r)\sin(\beta(r))\dot{\phi}(r, t) \end{bmatrix} \quad (5.11)$$

It should also be noted that the relative wind velocity $W(r, t)$ is defined at the first-quarter chord point from the leading edge. In addition to the above the wake vorticity generated by the blade motion induces a downward velocity of the wind on the airfoil which is referred as the downwash velocity. This velocity is normal to the chord line and it is applied at the third quarter chord point from the leading edge of the blade. The downwash velocity is equal to the upward component of the relative wind velocity imposed on the same point. Thus, the relative wind velocity is defined at the third-quarter chord point and henceforth, the torsional motion of the blade is introduced to the interaction term ' $u(r, t)$ ' as well. Here, the annotation ' $e_{3/4}(r)$ ' represents the distance between the aerodynamic center and third-quarter chord point, which can also be expressed in terms of the chord length as:

$$e_{3/4}(r) = \frac{1}{2}c(r) \quad (5.12)$$

The downwash velocity according to [3] is equal to :

$$W_\eta(r, t) = W_y\cos(\beta(r) + \phi(r, t)) - W_x\sin(\beta(r) + \phi(r, t)) \quad (5.13)$$

5.2. Wind Spectrum

The wind velocity profile is generally assumed to be composed of a mean velocity and a turbulence component fluctuating around the mean. The turbulence component is random in nature and therefore, it is usually generated from a standard wind spectrum. A wind spectrum is basically the frequency content of the wind velocity variation. One can also think of it as the energy content of the wind. Two most commonly adopted wind spectrum found in the literature are:

- Von Karman Turbulence Spectrum

$$\frac{fS_y(f)}{\sigma_y^2} = \frac{4fL_{2y}/W_y}{(1 + 70.8(fL_{2y}/W_y)^2)^{5/6}} \quad (5.14)$$

- Kaimal Turbulence Spectrum

$$\frac{fS_y(f)}{\sigma_y^2} = \frac{4fL_{1y}/W_y}{(1 + 6fL_{1y}/W_y)^{5/3}} \quad (5.15)$$

For this project, the Kaimal Turbulence Spectrum has been adopted for both the out-of-plane (longitudinal) and in-plane (lateral) direction of the rotor, since it fits the empirical

observations of atmospheric turbulence. The turbulence intensities and the length scales are referred from the Danish standard (DS 472, 1992) which is presented as:

$$I_x = 10\% \quad (5.16)$$

$$I_y = 0.8I_x \quad (5.17)$$

$$L_{1y} = 150m \quad (5.18)$$

$$L_{1x} = 0.3L_{1y} \quad (5.19)$$

Note that the axial component of the turbulence is not defined in this project since the axial degree of freedom of the blade has not been considered. Additionally, the mean wind velocities, also referred as steady flow velocities, adopted in the longitudinal and lateral directions are respectively presented as:

$$W_y = 11.4m/s \text{ (rated wind speed of the turbine)} \quad (5.20)$$

$$W_x = 0 \text{ m/s} \quad (5.21)$$

From the turbulence spectrum defined above, the time signal of the wind velocity in both the longitudinal and lateral directions can be generated through the following relation:

$$W(r, t) = W(r) + \sum_{k=1}^{N_f} \sqrt{2S_k(f)\Delta f_k} \cos(\omega_k t + \theta_k) \quad (5.22)$$

It is clear from Equation 5.22, that the wind velocity profile is composed of a mean velocity denoted by 'W(r n)', and a turbulence component represented by the second term, which is generated from the Kaimal Turbulence Spectrum.

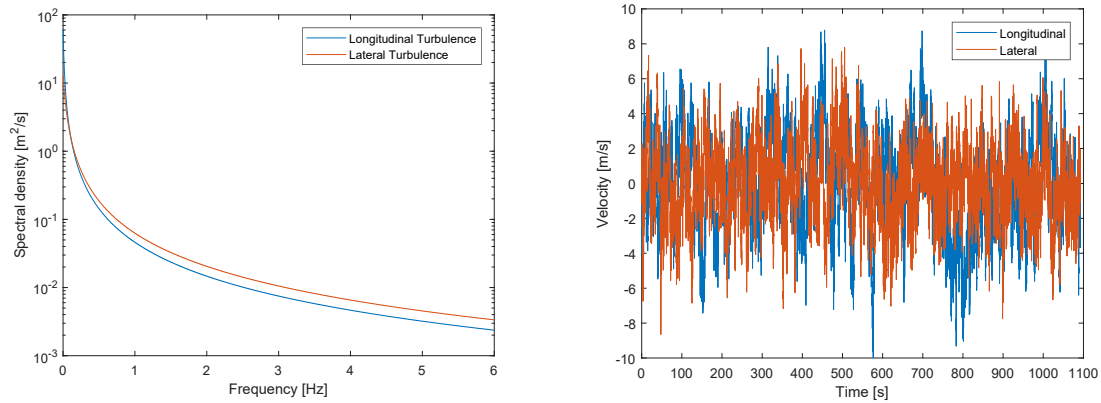


Figure 5.2: Kaimal Turbulence Spectrum in the longitudinal and lateral direction and the wind velocity fluctuation around the mean

6

Results and Discussion

After formulating the complete model in the previous chapters, this chapter presents the different cases studied after using the model. In total 8 cases were performed for each steady and unsteady flow separately for the model of the blade and the complete model of tower-blade. However, only relevant results are presented in this chapter. Especially for the tower only the operating blade case will be illustrated as it is of bigger interest. It should be noted that a viscous damping of 1% is accounted for in order to take into consideration the structural damping. When the wind turbine rotates 'pitched off', the pitch angle is 0 rad and when the wind turbine is standstill 'pitched on' the pitch angle is $\pi/2$ rad. The pitching of the blade is usually performed with respect to the nacelle and in reality, it has been done to avoid stalling of the wind flow by reducing the angle of attack. Apart from the pitching, the blade also exhibits pre-twist which contributes to the reduction of the angle of attack. Nevertheless, these are irrelevant for this model as the flow has been assumed to always remain attached.

Table 6.1: Operating Conditions of the wind turbine

Operating Condition	Rotational Speed (rpm)	Pitch Angle (rad)
Standstill	0	$\pi/2$
Rotating	12.1	0

6.1. Steady Flow

In order to get a better insight into the dynamic behavior of the blade, steady flow condition has been adopted, which can be obtained by dropping the turbulent component of the wind velocity, that is $\mathbf{w}(\mathbf{r}, \mathbf{t})$ in equation 5.7 .Moreover, due to the larger displacement at the blade tip (free end), the tip response has been considered for the purpose of analyzing the results.

6.1.1. Influence of gravity

Blade

Initially the effect of gravity on the blade will be observed. First of all the case of a rotating wind turbine is illustrated below.

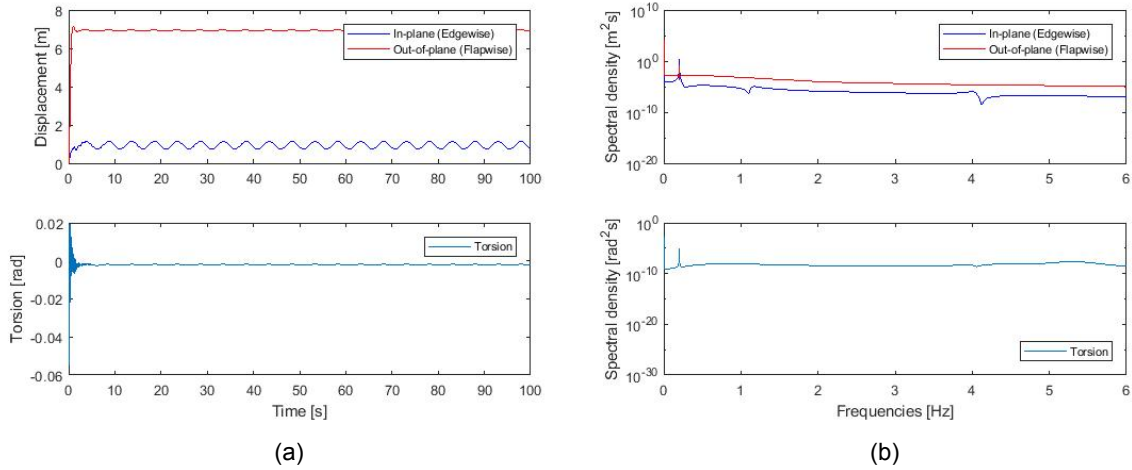


Figure 6.1: Influence of gravity on a rotating blade accounting both aerodynamic interaction and gravity

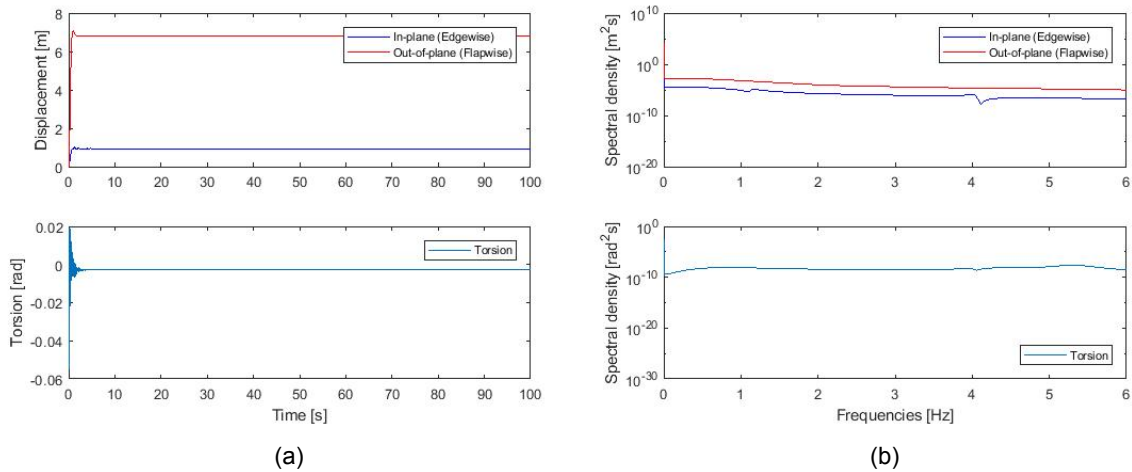


Figure 6.2: Influence of gravity on a rotating blade accounting only the aerodynamic interaction

It can be observed from the above graphs that the introduction of gravity induces an harmonic loading to the blade as seen on figure 6.1a. This harmonic load varies with the rotation of the blade and as a result the harmonic motion persists in time. In addition to that it can be observed a peak at the spectral density plot 6.1b corresponding to the rotational velocity of the blade (12.1rpm=0.2 Hz), which is associated with the harmonic motion of the blade introduced by gravity. In addition to the above it should be noted that the rotating blade deflects on the positive out-of plane direction mainly which perfectly agrees with the

definition of the lift force, see figure 5.1. It worths noting that the displacement in the out of plane direction is almost 8m which is totally in line with [3]. Also when comparing figures 6.1b and 6.2b it is obvious that the gravity does not effect the structural modes.

However the gravity does not have the same influence on a standstill blade.

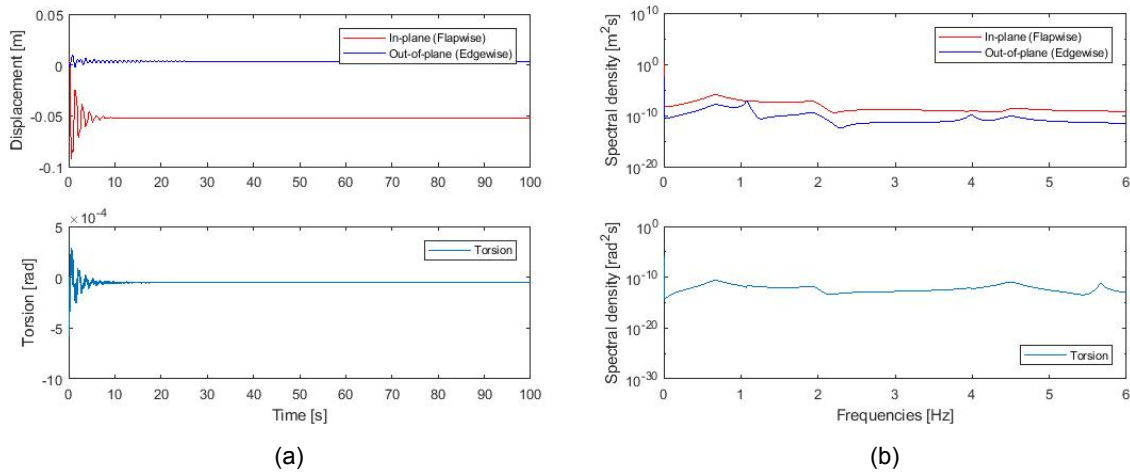


Figure 6.3: Influence of gravity on a standstill blade accounting both the aerodynamic interaction and the gravity

In this specific case the blade is pitched on which results in interchanging the flapwise with the edgewise motion with respect to the rotor plane. It is observed that the harmonic motion due to the gravity does not exist, which is due to the fact that the harmonic load in this case is a static load. Due to the fact that the blade is practically not rotating, the deflections in both in plane and out of plane directions are significantly reduced 6.3a. This is because the lift force is significantly reduced as the angle of attack becomes very small since the blade is almost parallel to the flow. In addition to the above it should be noted that since the displacements are so small, thus the damping is small.

Tower

As mentioned in previous chapters in order to make the model more realistic the tower was introduced to the blade and an aerodynamic analysis was performed on that model too. First of all, the effect of gravity was observed.

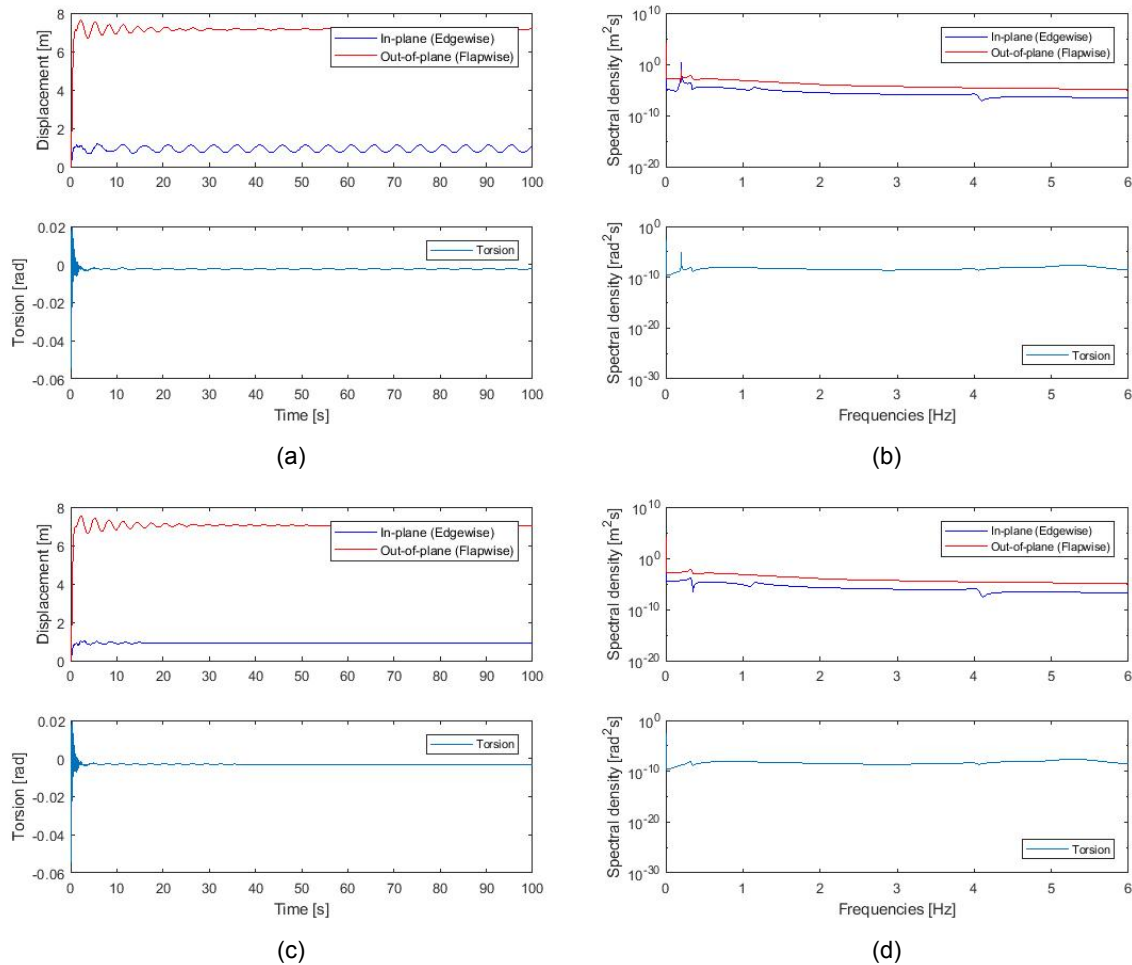


Figure 6.4: Influence of gravity on a rotating blade with tower a) and b) taking into account both gravity and aerodynamic interaction, while c) and d) represent the same but without considering gravity

First of all when comparing figures 6.4a and 6.1a it is observed, especially on the flapwise-out of plane direction a small added vibration to the blade tip response. This vibration exists due to the added force that is derived from the stiffness of the tower. As mentioned in equation 2.41 the first term on the second line represents the force due to the stiffness of the tower which is responsible for that vibration. In addition to the above when comparing figures 6.4b and 6.1b it is obvious that except for the resonance peak at 0.2 Hz, a small peak at around 0.3 Hz (first fore-aft natural frequency of the tower) is observed, however it is damped due to the aerodynamic interaction. As mentioned before there still a vibrational motion especially on the edgewise direction due to the gravity.

6.1.2. Influence of Aerodynamic Interaction Blade

The aerodynamic Lift and drag forces are coupled to the structural response velocity $\dot{\mathbf{u}}(r,t)$, which introduces an additional aerodynamic damping, to the blade response. An additional mass is also added to the blade through the inertia force $\mathbf{F}_I(r,t)$, m which depends on the blade response acceleration. The significance of this damping is obvious in the following figures.

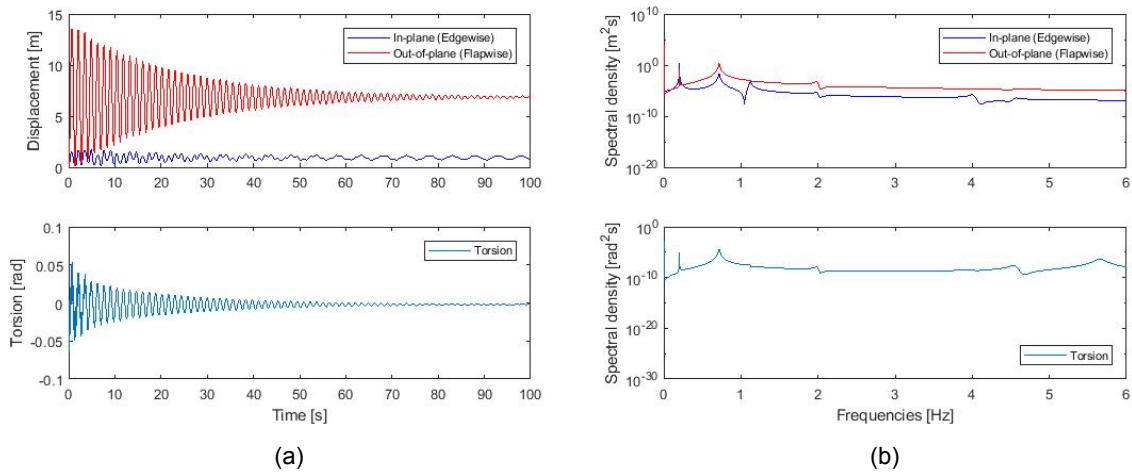


Figure 6.5: Influence of aerodynamic interaction on a rotating blade accounting only the gravity

When comparing figures 6.1a and 6.5a it is obvious that the blade tip response reduces significantly when considering the aerodynamic interaction due to the aerodynamic damping. Also when comparing the spectral density plots 6.1b and 6.5b it is obvious that when considering the aerodynamic interaction the resonance peaks are flatter. Especially the peaks corresponding to the flapwise modes are more damped since the response in the flapwise direction is bigger.

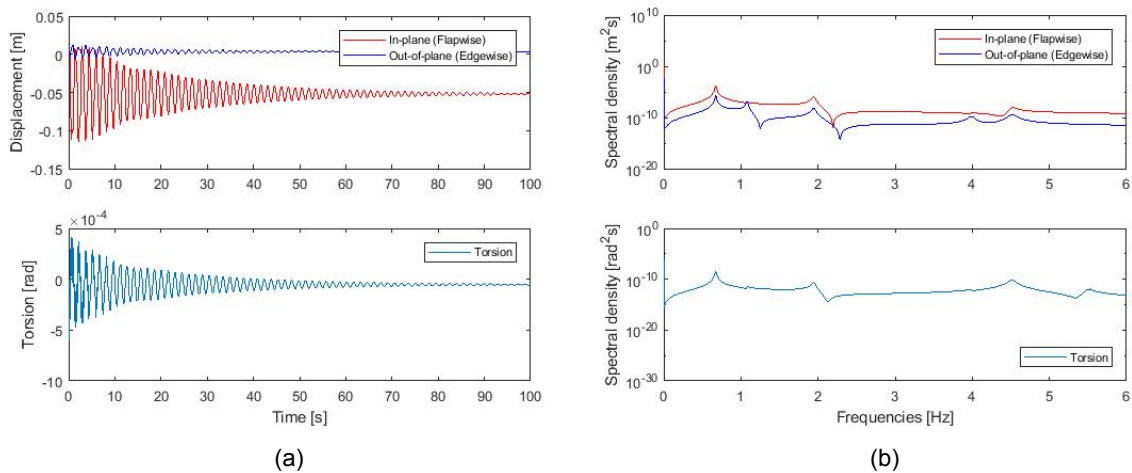


Figure 6.6: Influence of aerodynamic interaction on a standstill blade accounting only the gravity

When observing figures 6.3a and 6.6a it is obvious again that when considering the aerodynamic interaction the blade tip response is damped, however the magnitudes of the responses are generally smaller in this case, the reasons for which are explained previously.

Tower

In addition to the above the effect of aerodynamic interaction on the complete model will be observed.

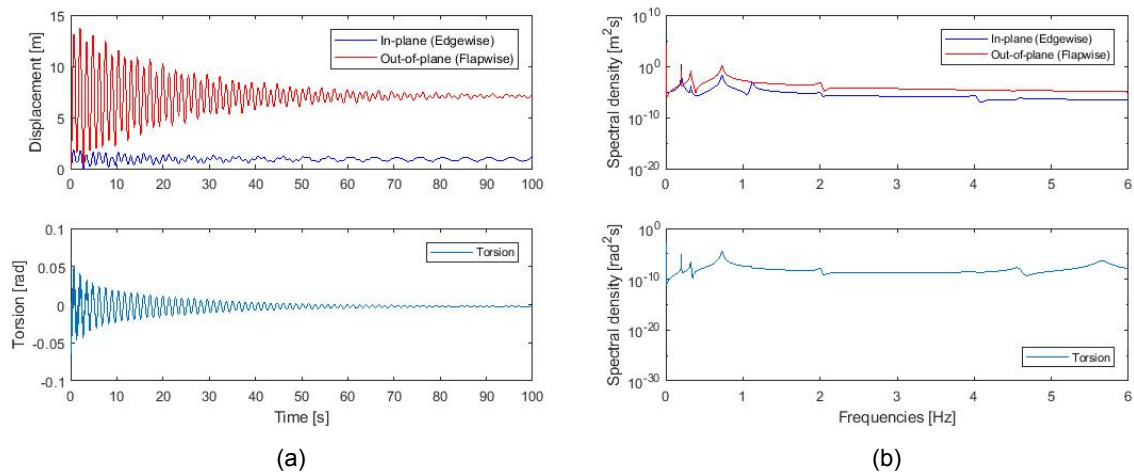


Figure 6.7: Influence of aerodynamic interaction on a rotating blade with tower taking into account only gravity

When comparing figures 6.4a and 6.7a it is obvious that when considering the aerodynamic interaction even when taking into account the tower still the blade tip response is severely damped especially the flapwise direction. In addition to the above a general observation is that again in the flapwise direction an extra vibration is observed due to the tower. As far as the spectral density plots are concerned, when the aerodynamic interaction is not considered the resonance peak at the natural frequency of the tower is more prominent due to the lack of aerodynamic damping. Another observation is that in figure 6.7b the resonance peaks are less flat than figure 6.4b again due to the lack of aerodynamic damping.

Effect of Tower on Blade Tip Response

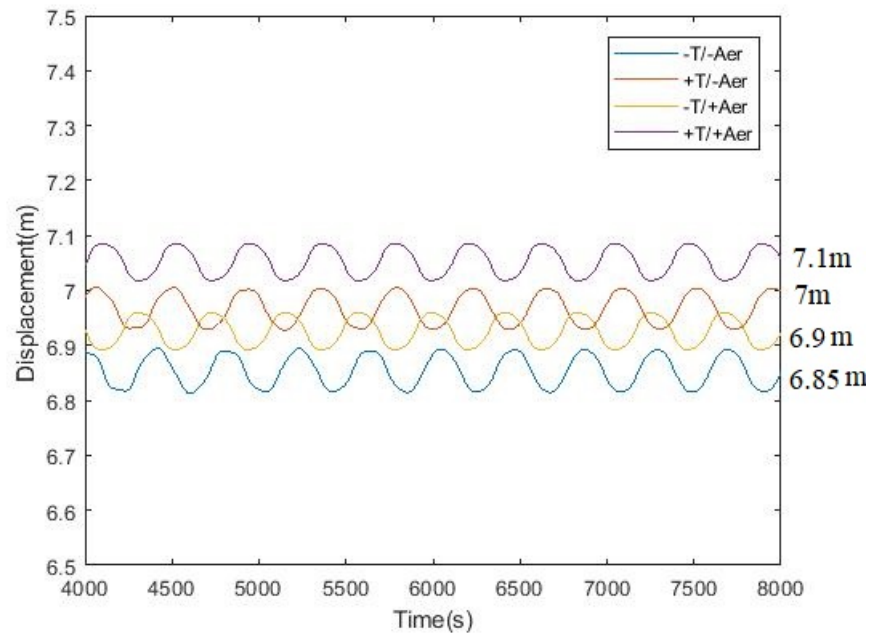


Figure 6.8: Effect of tower on blade tip response -comparison between the cases with/without tower considering only gravity (blue and red line)- comparison between the cases with/without tower considering both gravity and aerodynamic interaction (yellow and purple line)

In order to assess the effect of tower on blade tip response different initial conditions were utilized. The response of the blade for fully developed speed ($11,4 \text{ m/s}$) was utilized as initial condition. As a result the transient response was eliminated vastly. However the time window that is represented is from 4000 to 8000 seconds in order to have no effect of the transient response.

When observing figure 6.8 and more specifically the blue and red line, which do not consider aerodynamic interaction, it is clear that the tower induces an extra displacement to the blade response equal to 0.15m . Correspondingly when considering aerodynamic interaction (yellow and purple line) the tower induces a displacement equal to 0.2m . It is expected that the tower will induce an added displacement to the blade as the spring force, due to tower stiffness, induces a displacement.

6.2. Unsteady Flow

In this section the fluctuation of the wind velocity $\mathbf{w}(r,t)$ will be taken into account and its effect on the blade will be analyzed.

6.2.1. Influence of gravity

Blade

Initially the effect of gravity on a rotating blade will be observed.

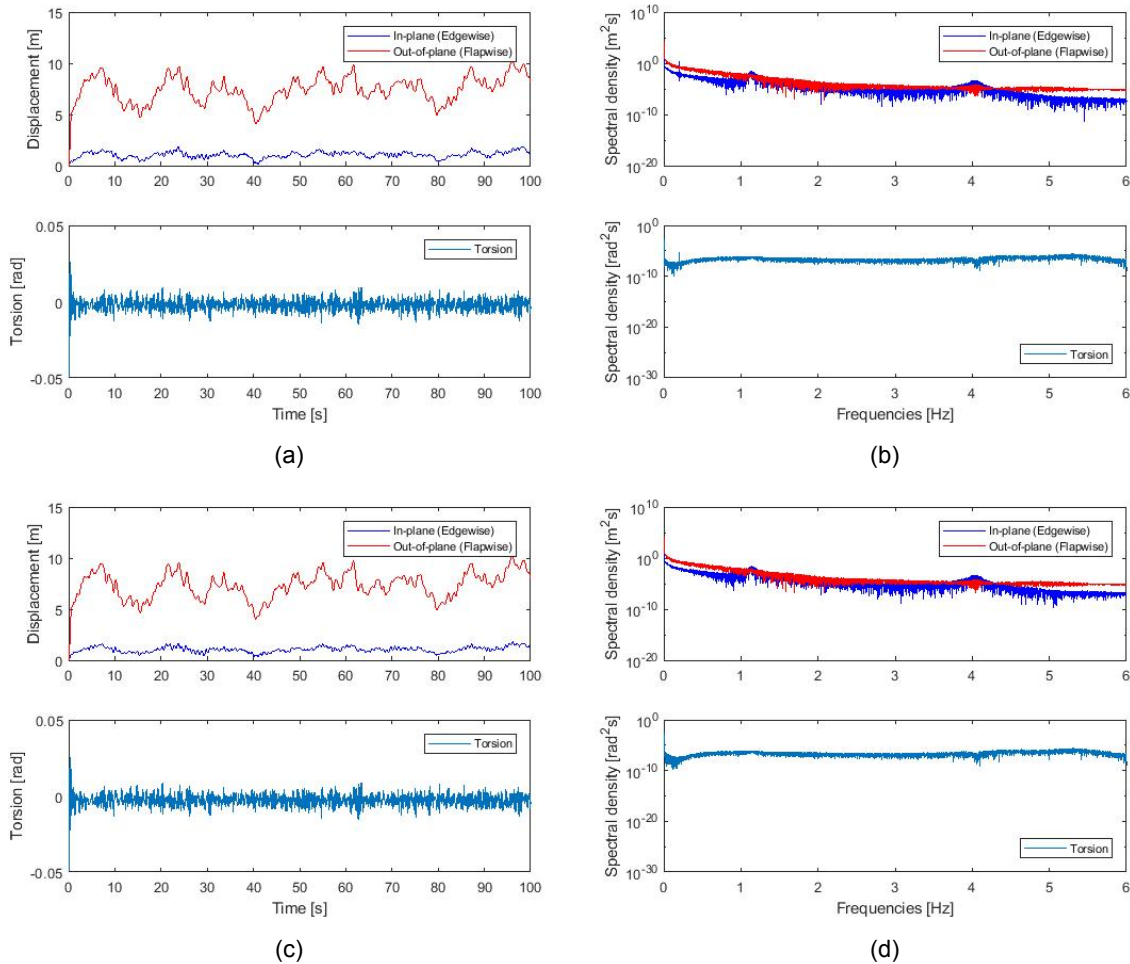


Figure 6.9: Influence of gravity on a rotating blade a) and b) taking into account both gravity and aerodynamic interaction, while c) and d) represent the same but without considering gravity

A general observation for the unsteady flow is that the blade tip response does not obtain a steady state solution as seen due to the fluctuation of the wind. Another observation is that the gravity again induces a harmonic loading which is obvious on figure 6.9a, especially on the in-plane(edgewise) direction. In addition this effect is obvious on the spectral density plot 6.9b as there is a resonance peak at 0.2 Hz which as mentioned before corresponds to the rotational velocity of the blade. Another observation between figures 6.9b and 6.9d, when comparing the resonance peaks of in-plane and out of plane directions, is that the in plane modes are less damped than the out of plane modes, since there is more damping on the out of plane direction due to the existing bigger blade tip response .

Following the effect of gravity on the standstill blade will be represented.

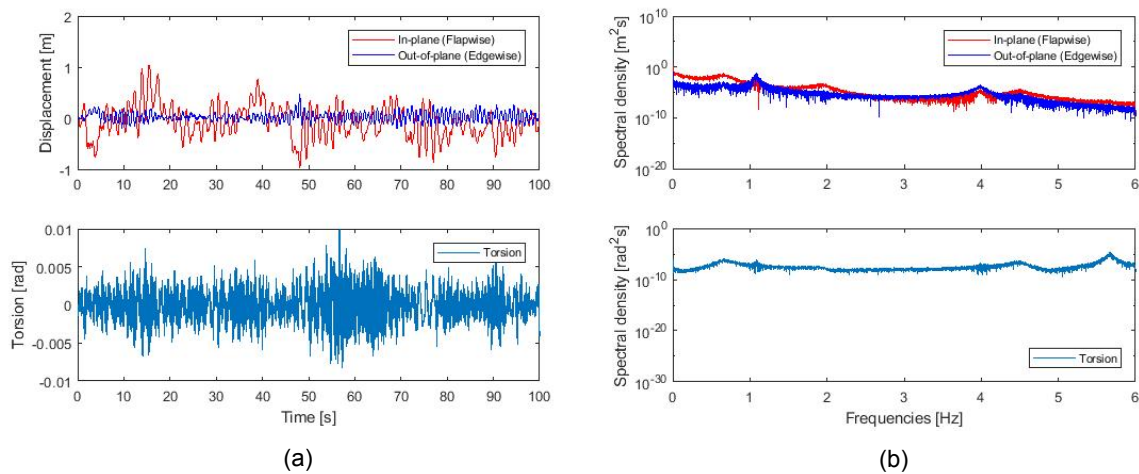


Figure 6.10: Influence of gravity on a standstill blade accounting both the aerodynamic interaction and gravity

In this case the influence of gravity is not obvious on the spectral density plot, However it is obvious on the torsional blade tip displacement as the mean of the displacement is transferred. This offset is due to the eccentricity of the center of mass from the elastic axis which induces a torque around the corresponding axis. Another observation is that the blade tip response in figure 6.10a is bigger than the magnitude of the response in figure 6.3a. This is due to the fact that the response of the standstill blade due to the lack of rotational velocity, is affected more by the wind fluctuation as seen on equation 5.11. When the turbulence component is added, the wind velocity that reaches the blade is higher leading to an increased blade tip response. In the operating case of the blade the response is also increased after inducing turbulent flow, however the difference is not so severe due to the fact that the influence of the rotational velocity is bigger compared to the turbulent velocity component.

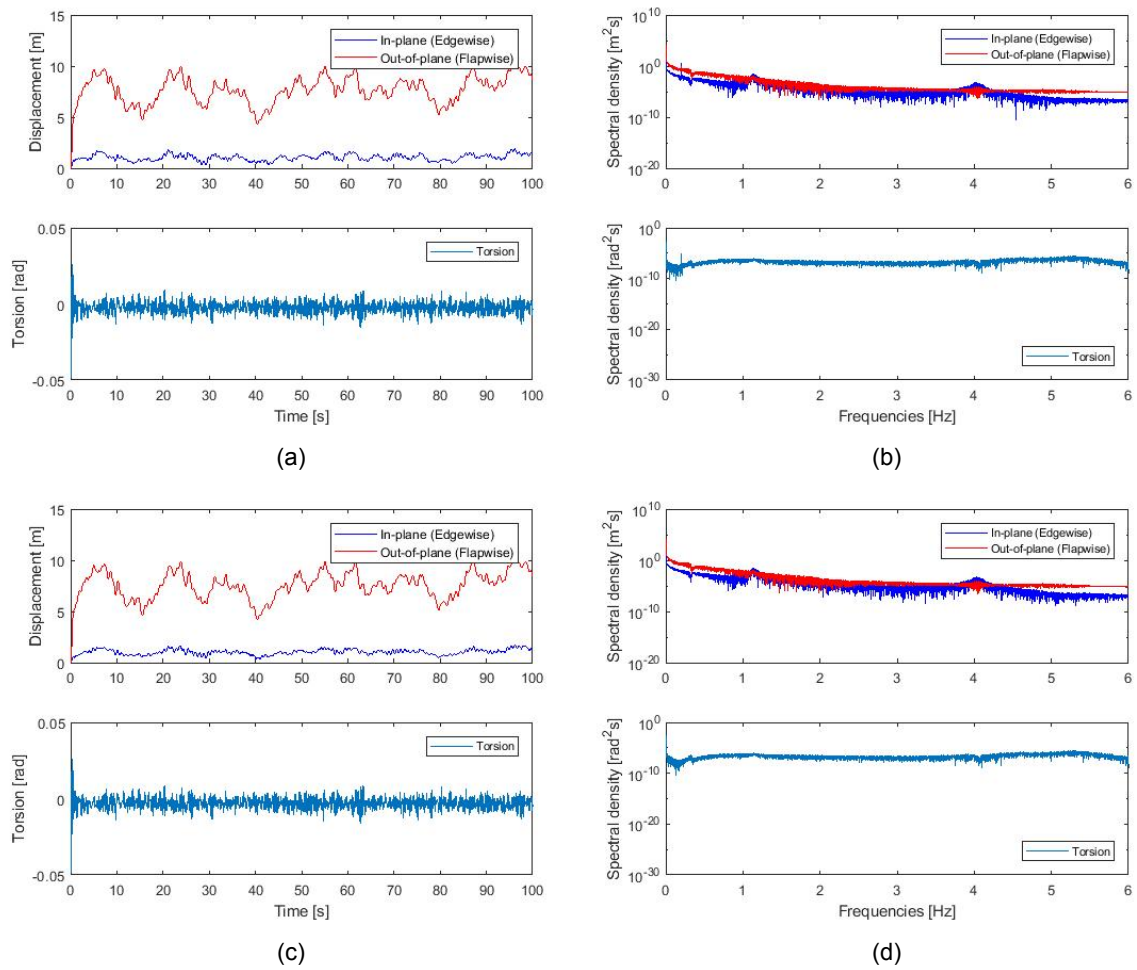
Tower

Figure 6.11: Influence of gravity on a rotating blade with tower a) and b) taking into account both gravity and aerodynamic interaction, while c) and d) represent the same but without considering gravity

It is obvious from figure 6.11a that the gravity induces again a harmonic load to the system and a resonance peak at around 0.2 Hz due to the gravity is observed on figure 6.11b.

6.2.2. Influence of Aerodynamic Interaction Blade

Initially the influence of aerodynamic interaction under unsteady flow, on a rotating blade is going to be observed.

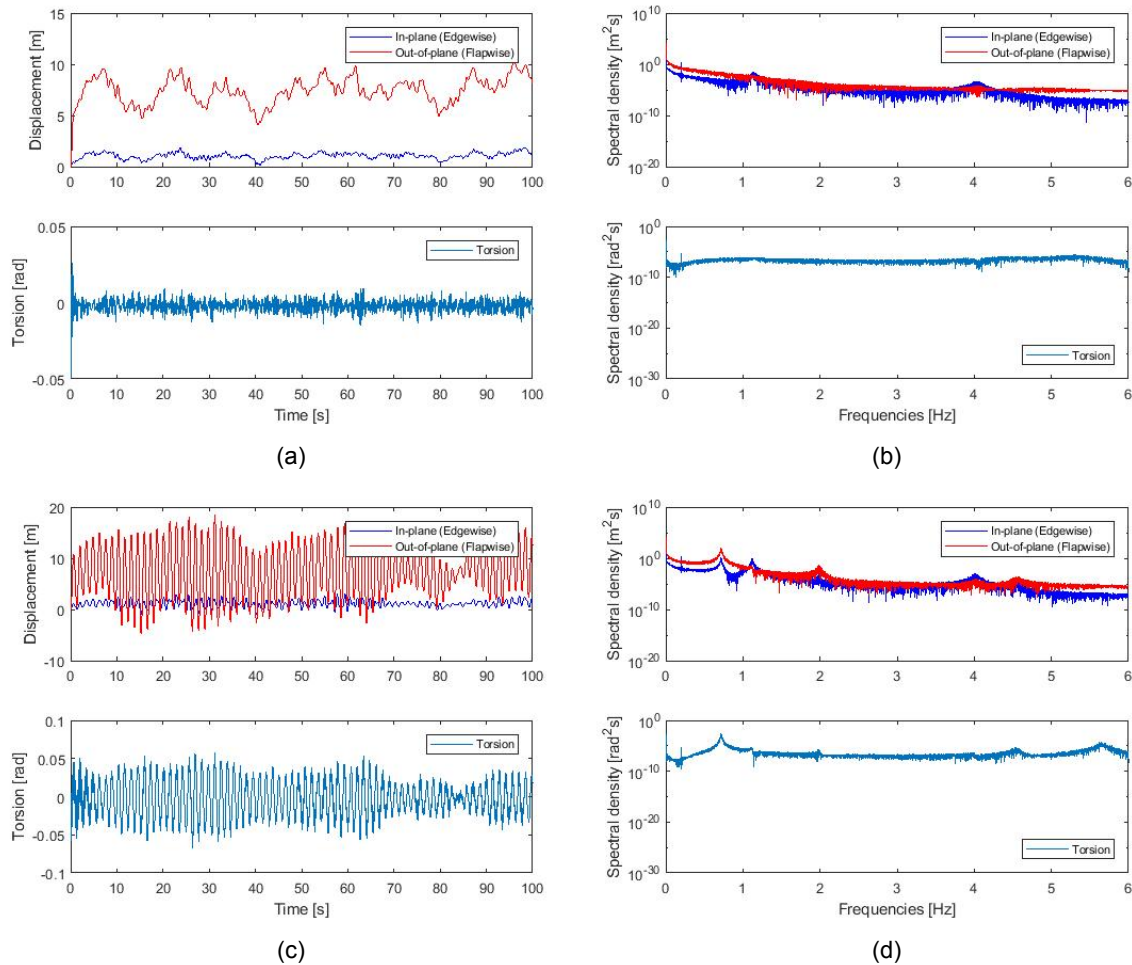


Figure 6.12: Influence of aerodynamic interaction on a rotating blade a) and b) taking into account both gravity and aerodynamic interaction, while c) and d) represent the same but without considering the aerodynamic interaction

From figures 6.12a and 6.12c it is obvious that after adding the aerodynamic interaction the blade tip response is vastly damped and especially the out-of plane tip displacement. This is in agreement with the spectral density plots 6.12b and 6.12d, in which the peaks of out-of plane blade tip response are more damped than those of the in-plane blade tip response.

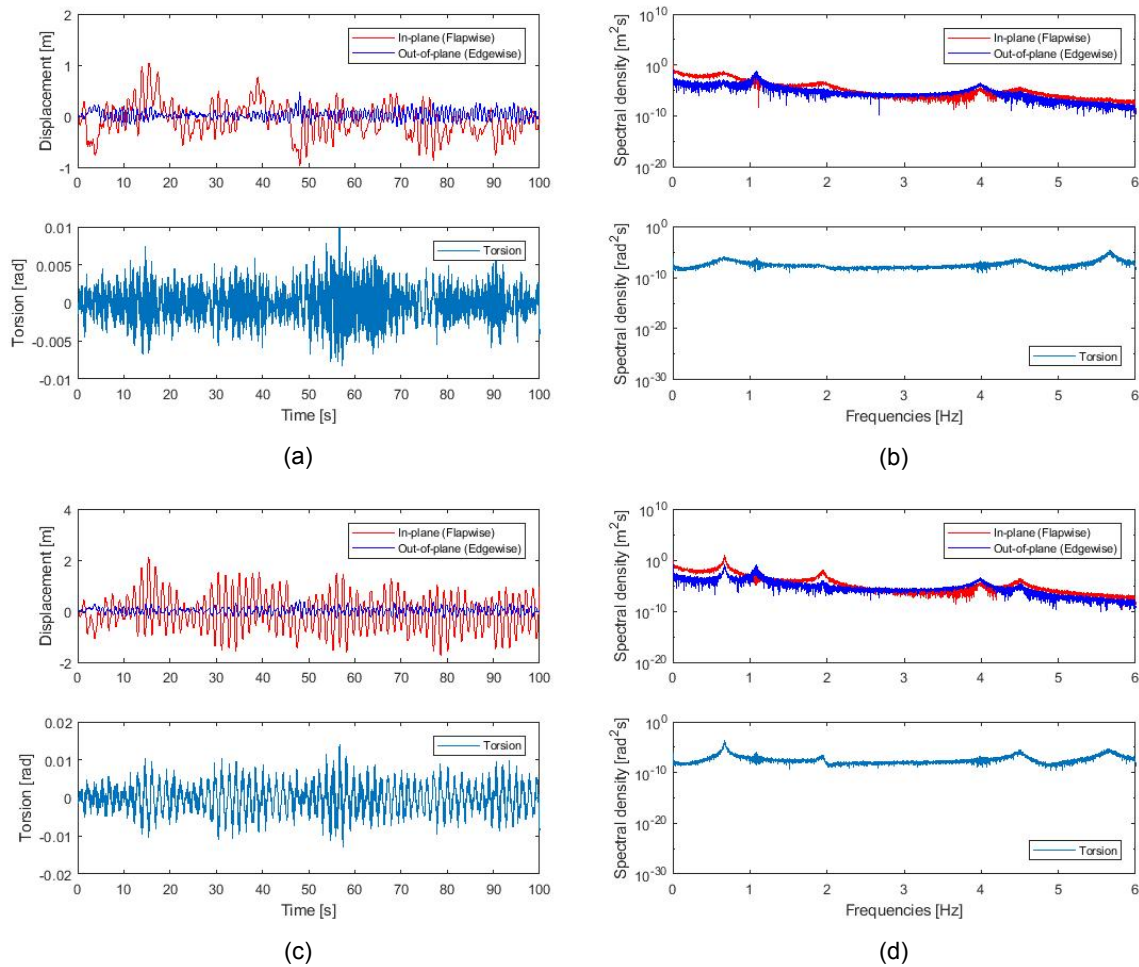


Figure 6.13: Influence of aerodynamic interaction on a standstill blade a) and b) taking into account both gravity and aerodynamic interaction, while c) and d) represent the same but without considering the aerodynamic interaction

It is also here observed that when the aerodynamic interaction is taken into account the blade tip response is damped. However the torsional direction does not seem to be affected severely. In addition to the above when observing figures 6.12b and 6.13b it is obvious that after applying the aerodynamic damping, the torsional spectral density plot still presents resonance on the flapwise structural modes, a scenario which is not valid for the edgewise modes. As a result it can be concluded that the torsional-flapwise coupling is more dominant than the torsional-edgewise coupling, which is also obvious from the structural modes. This is logical since the flapwise direction is more sensitive due to its lower stiffness, thus influencing the torsional mode more.

Tower

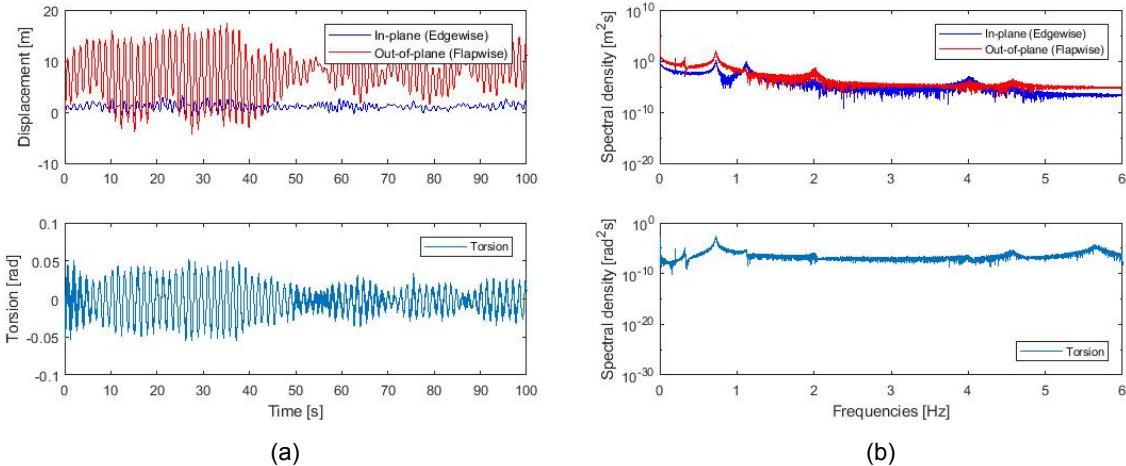


Figure 6.14: Influence of aerodynamic interaction on a rotating blade with tower taking into account only gravity

Comparing figures 6.11a and 6.14a it is obvious like in the blade that the response especially in the flapwise direction is damped due to the aerodynamic interaction. The torsional direction is also damped due to the more intense coupling between the flapwise and the torsional direction. As far as the spectral density plots are concerned the observations are similar to the steady flow.

6.3. Tower Shadow Effect

In order to create a more realistic model the tower shadow effect will be also taken into account. Tower shadow effect is the blocking of the air flow by the tower which results in regions of reduced wind speed both upwind and downwind of the tower. This reduction is more severe for tubular towers than for lattice towers and, in the case of tubular towers, is larger on the downwind side because of flow separation. As a consequence the downwind case of tower shadow will be also modeled in order to observe the effect more clearly. The tower shadow effect downwind of the wind turbine was modeled by [26] and [27]. [27] performed experiments which gave the velocity contours downwind an octagonal tower with diameter 12.2 cm. It was found that around 4 to 5 tower diameters (dependent on the surface of the tower that points towards the flow) downwind the tower the velocity is zero. However, the tower used in [27] is octagonal which affects the velocity contours. [26] modeled tower shadow for a 5 MW wind turbine for 3 and 6 tower diameters behind the tower, which is more relevant to this research. It should be noted that the way the tower shadow is modeled is simple and ideally experiments could have been done in order to obtain the velocity contour behind one tower diameter of a scaled cylindrical tower. In addition the flow is chosen to be modeled at one tower diameter since the overhang distance is 5 m which is almost equal to one tower diameter.

Upwind Tower Shadow Effect

The velocity deficit upwind of a tubular tower can be modeled using potential flow theory according to [25]. The flow around a cylindrical tower is derived by superposing a doublet, i.e., a source and sink at very close spacing, on a uniform flow giving the stream function:

$$\psi = U_{\infty}y\left(1 - \frac{(D/2)^2}{x^2 + y^2}\right) \quad (6.1)$$

where D is the tower diameter, and x and y are the longitudinal and lateral coordinates with respect to the tower center according to figure 6.16. Differentiation of ψ with respect to y yields the following expression for the flow velocity in the x direction:

$$U = U_{\infty}\left(1 - \frac{(D/2)^2(x^2 - y^2)}{(x^2 + y^2)^2}\right) \quad (6.2)$$

The second term within the brackets is the velocity deficit as a proportion of the undisturbed wind speed.

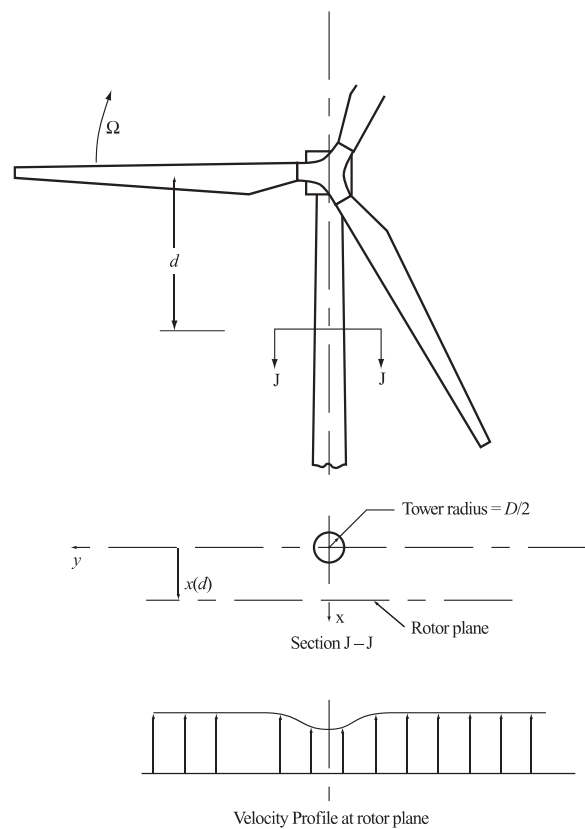


Figure 6.15: Tower Shadow Parameters according to [25]

Downwind Tower Shadow Effect

According to [26] and [27] the velocity profile of tower shadow on a downwind wind turbine is modeled by the following formula :

$$U = U_{\infty} \left(1 - \Delta \cos^2 \frac{y\pi}{wd} \right) \quad (6.3)$$

Where :

- Δ is the velocity deficit in the middle of the wake. For that specific parameter there is not a specific mathematical formula from which it could be calculated. Usually this parameter is chosen to be around 40% but this is only based on empirical measurements. According to [26] the velocity profile is optimally modeled with a velocity deficit of 20% at a distance equal to 3 tower diameters behind the tower and 10% at 6 tower diameters behind the tower. However in this specific case the considered distance is 5m (overhang distance for 5MW NREL) which is almost one tower diameter behind the tower. Assuming that the velocity deficit at exactly zero distance from the tower will be 100% and considering the data mentioned above, utilizing polynomial interpolation the velocity deficit is found to be 66%.

- w is a dimensionless parameter dependent on the cylinder diameter D and the physical wake width W and is equal to :

$$w = \frac{W}{2D} \quad (6.4)$$

The velocity profile according to [26] is optimally modeled at a distance equal to 3 tower diameters utilizing physical wake width $W=1.8$ tower diameters and at a distance 6 tower diameters for $W=2.3$ tower diameters. Since the wake profile (approximately) has a cone shape, linear interpolation was utilized and the physical wake width at one tower diameter distance is equal to 1.27 tower diameters.

- x is the distance between the tower and the rotor
- d is the total width of the deficit region (for computational reasons was accounted to be equal to the number of elements of the model).

Using formulas 6.2 and 6.3 the velocity profiles are illustrated below.

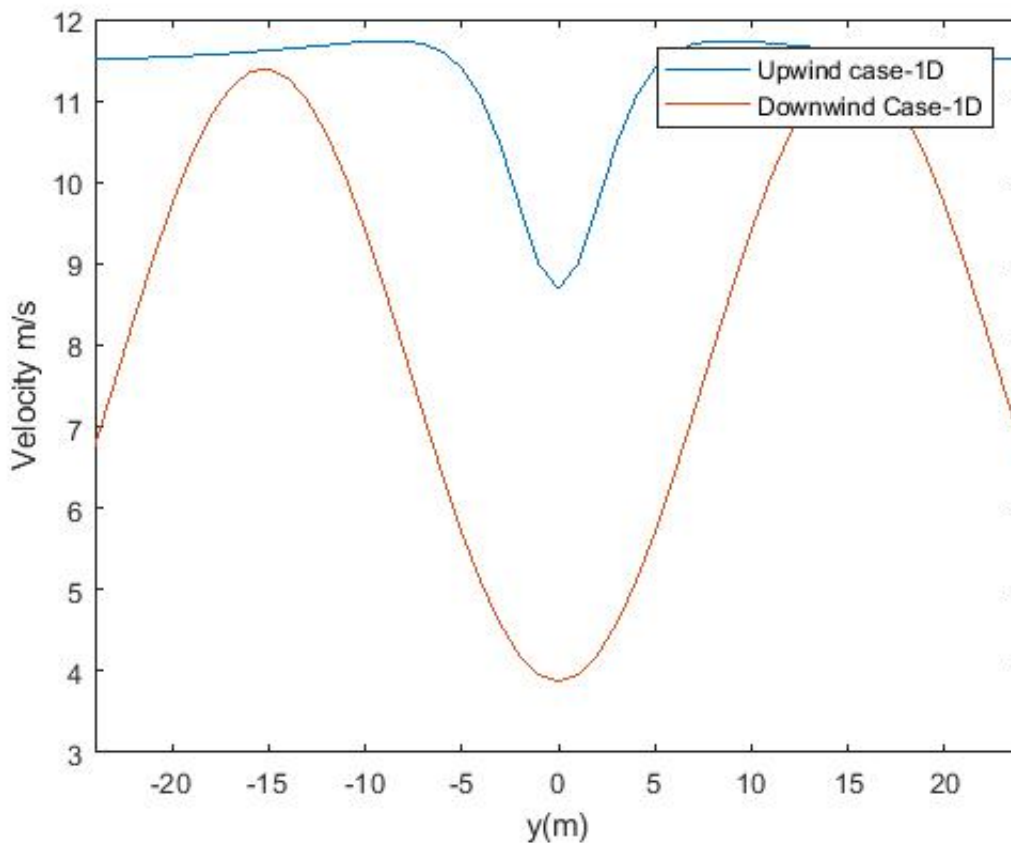


Figure 6.16: Velocity Profile due to Tower Shadow-Upwind versus Downwind case

Figure 6.16 represents the velocity deficit for the upwind and downwind case at a distance equal to one tower diameter. It is obvious that the velocity deficit in the downwind case is bigger, which is logical since the flow has passed the tower. Afterwards analysis was performed for the cases of upwind and downwind tower shadow taking into account steady and unsteady flow conditions. For relevance reasons only the results for the rotating model will be presented. The rotating blade is of more interest since there is bigger blade response, hence the tower shadow effect will be more obvious. The rotational velocity of the blade is 12.1 rpm and the pitch angle is 0 deg. The wind conditions are the same as stated in section 5.2.

6.3.1. Steady Flow

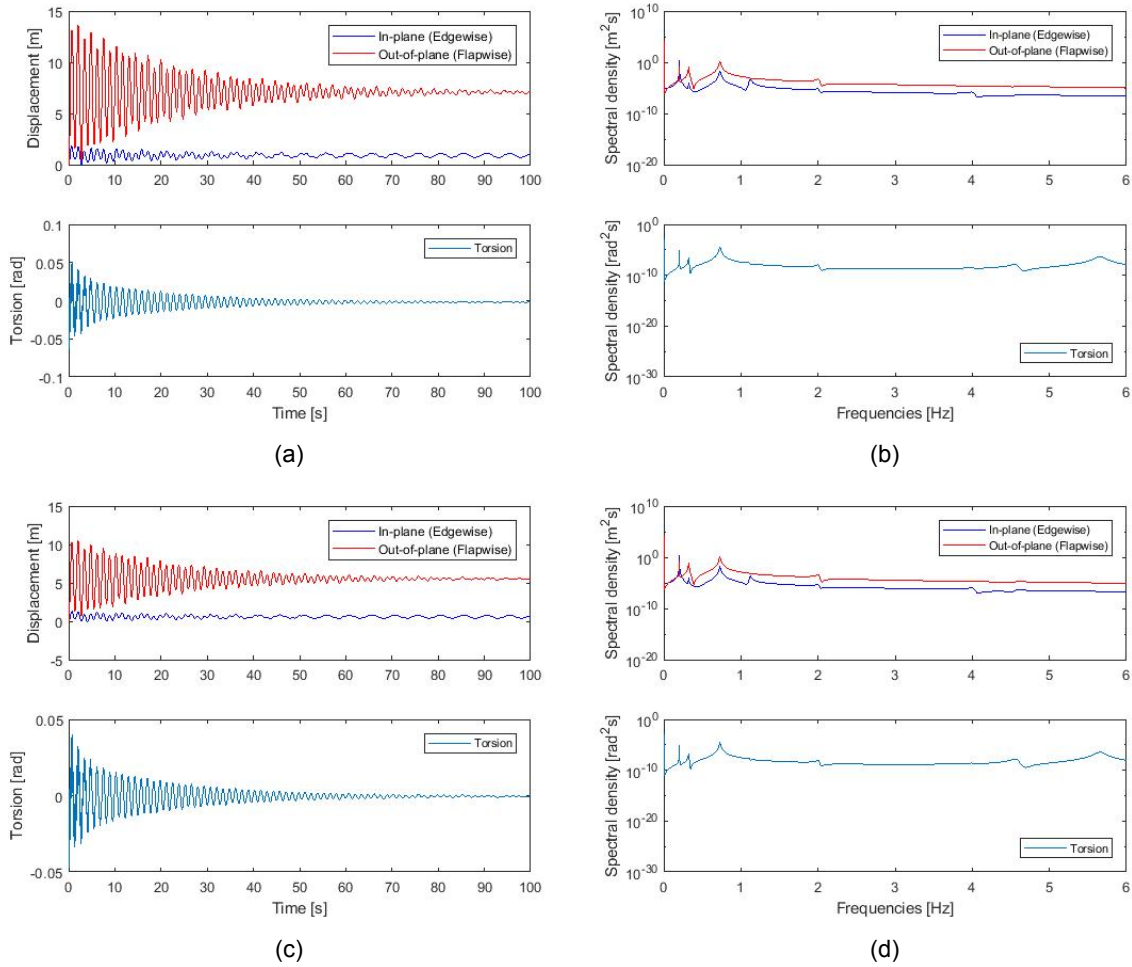


Figure 6.17: Blade tip response without aerodynamic interaction considering gravity a) and b) upwind tower shadow effect while c) and d) represent the same but considering downwind tower shadow effect

When comparing figures 6.17a and 6.17c with 6.7a, before considering tower shadow it is obvious that the shape of the blade tip response is similar however the amplitude of response especially on the downwind case is reduced. When comparing figures 6.17a and 6.7a it is obvious that the blade tip response amplitude is almost identical in both cases which is in line with what was mentioned previously that the effect of tower shadow on an upwind wind turbine is small. However when comparing figures 6.17c and 6.7a it is obvious that the blade tip response on the downwind case is damped especially in the flapwise direction and torsion which is in line with the fact that since the flow passes first from the tower, the shadow effect will be more intense on the blade.

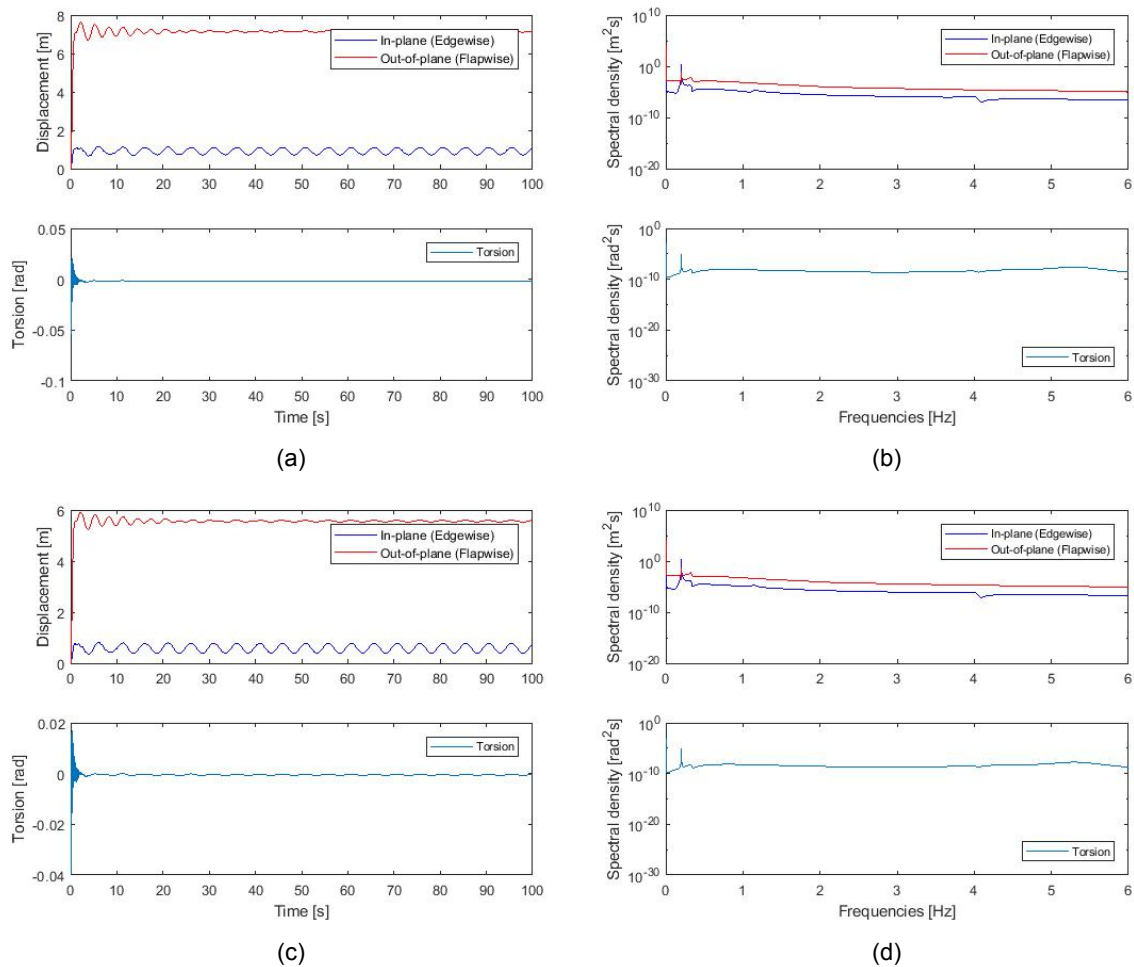


Figure 6.18: Blade tip response considering both aerodynamic interaction and gravity a) and b) upwind tower shadow effect while c) and d) represent the same but considering downwind tower shadow effect

When comparing figures 6.4a and 6.18a it is again obvious that the effect of tower shadow on the upwind case is almost negligible. On the other hand on figure 6.18c the responses are smaller due to the downwind tower shadow (from almost 8 m the blade tip response is below 6 m after the tower shadow)

In order to assess more clearly the tower shadow effect different initial conditions were utilized. The response of the blade for fully developed speed (11,4 m/s) was utilized as initial condition. As a result the transient response was eliminated vastly. However the time window that is represented is from 4000 to 8000 seconds in order to have no effect of the transient response.

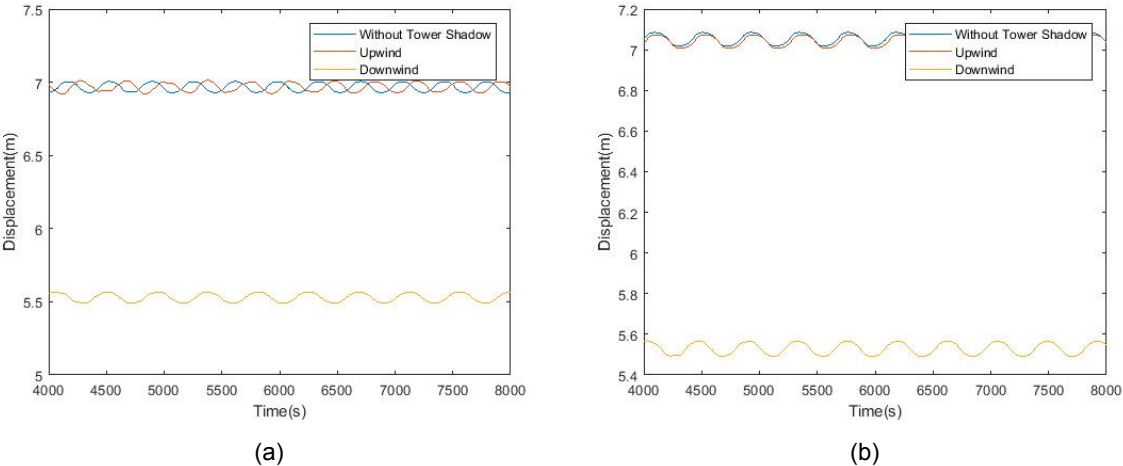


Figure 6.19: Influence of tower shadow a) on a rotating blade with tower taking into account only gravity b) on a rotating blade with tower considering both aerodynamic interaction and gravity

It is obvious from figures 6.19a and 6.19b that in both cases the effect of downwind tower shadow damps the blade tip response vastly and the calculated reduction is about 21%. The same does not hold for the upwind tower shadow, since it is obvious that the responses are almost the same. This corresponds to reality as the flow in the upwind case passes first from the rotor and then from the tower.

6.3.2. Unsteady Flow

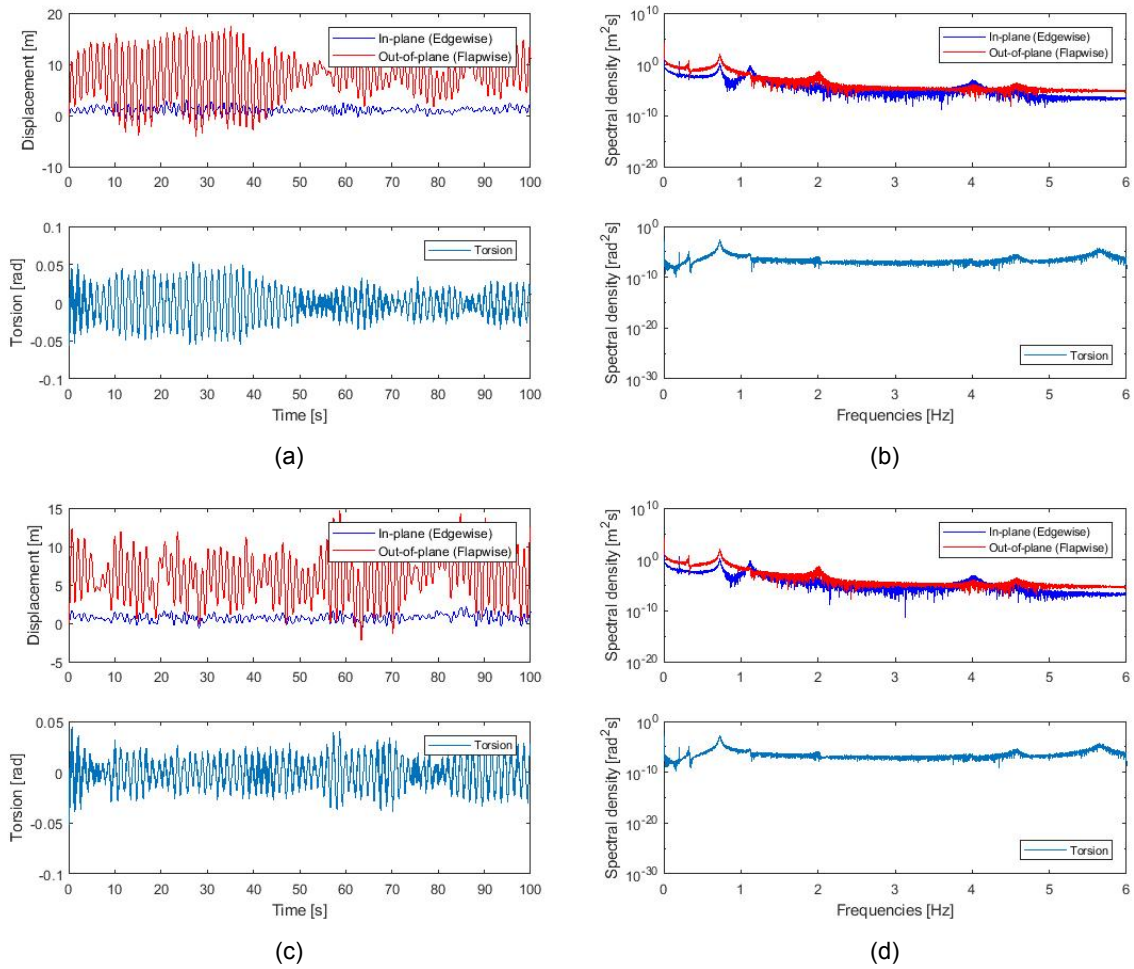


Figure 6.20: Blade tip response without aerodynamic interaction considering gravity a) and b) upwind tower shadow effect while c) and d) represent the same but considering downwind tower shadow effect

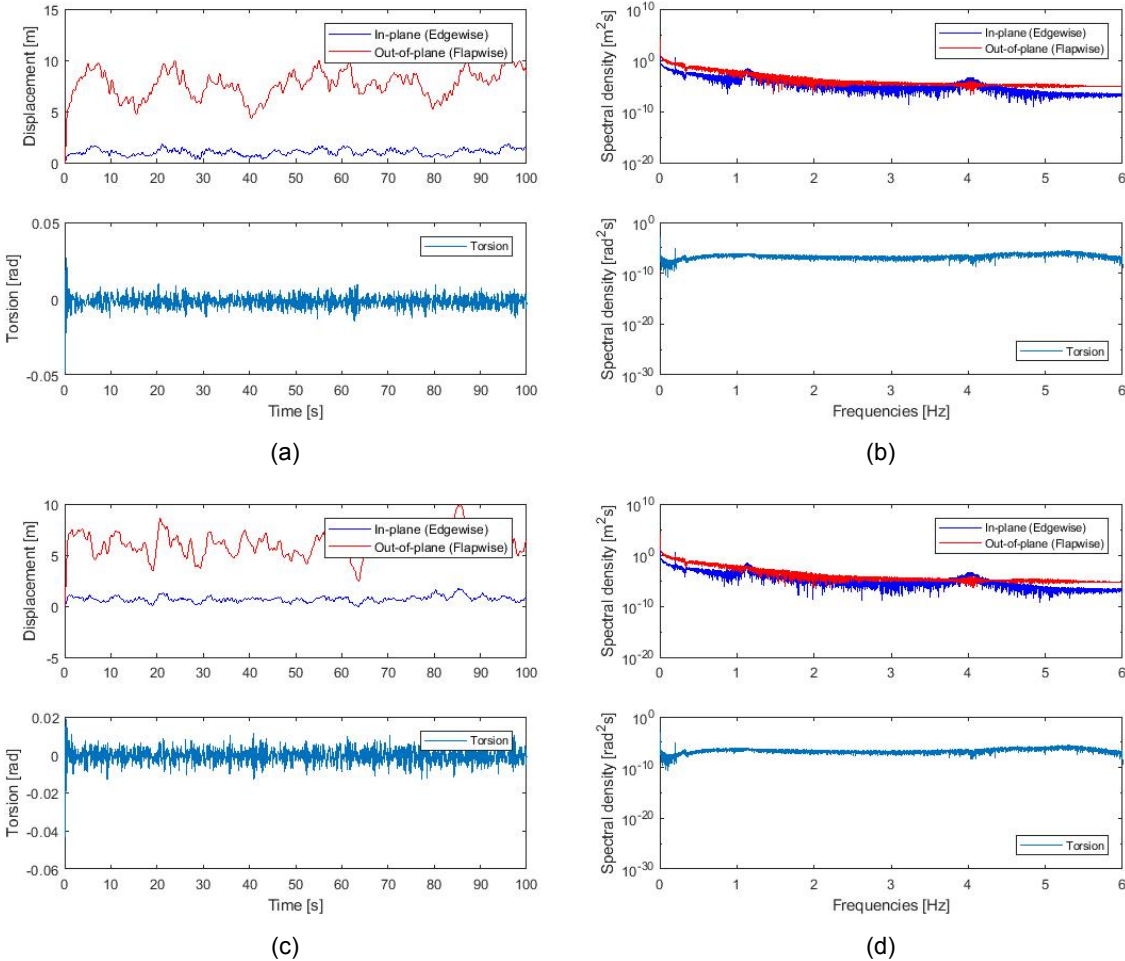


Figure 6.21: Blade tip response considering both aerodynamic interaction and gravity a) and b) upwind tower shadow effect while c) and d) represent the same but considering downwind tower shadow effect

In the unsteady flow it is again obvious that the blade tip response is smaller in the case of downwind tower shadow as expected.

Conclusions and Recommendations

7.1. Conclusions

Based on the research questions formulated in section 1.4 the following conclusions are drawn:

- The effect of the tower on the structural behavior of the blade as mentioned before does not agree with expectations. The inclusion of the tower (as an extra degree of freedom to the system) induces a slight stiffening effect to the blade, in contradiction to expectations. In order to accurate this fact a simpler 2 DOF system was constructed and its structural behavior was found similar to the behavior of the blade with the tower justifying the stiffening effect.
- The blade response is severely affected by the tower, since, as observed from the graphs in previous chapters, the tower induces an extra harmonic vibration on the flapwise direction .This originates from the added force due to the stiffness of the tower
- Adding the tower shadow effect lowers the blade tip response, affecting consequently the amount of wind energy transformed to electric energy. This has severe consequences on the productivity of the wind farm.
- The downwind shadow effect is more severe on the blade tip response compared to the upwind case. This is in total agreement with the literature which states that since the flow passes first from the tower, the shadow effect will be more severe when the flow reaches the blade.

7.2. Recommendations

This work is an attempt to understand the effect of tower shadow under different cases. It is expected that more knowledge in the future can add more accuracy to this study. Some of the fields that could be analyzed in more depth are:

- The tower could be modeled as an Euler-Bernoulli beam and not like a mass with stiffness. This would show more realistically the effect of the tower on the blade and also the model would be more accurate.
- The aerodynamic loads are assumed to be steady with time, which in reality is not true as the definition of lift force is not valid in unsteady aerodynamics. Thus the unsteady flow could be modeled more realistically in the future.
- Another interesting aspect would be to conduct an economic analysis on productivity of the system before and after tower shadow for downwind and upwind case. This could lead to valuable results which could be used in the optimization of wind farms.
- In addition, a foundation analysis could be conducted, in order to assess the aerodynamic loads that the wind turbine can withstand.
- In order to construct a more realistic wind profile, a rotationally sampled spectrum could be used as it is more suitable for the operating condition of the blade.
- The tower shadow is modeled quite simply in this specific project due to lack of numerical data. Further analysis could be done in finite element software where the flow could be modeled more realistically. In addition experiments could be done, and the numerical data from the tower shadow profile could be used as input in this specific model.

Bibliography

- [1] B. S. Kallestøe, (2007 May) *"Equations of Motion for a Rotor Blade, Including Gravity, Pitch Action and Rotor Speed Variations"*, WIND ENERGY 10, 209-230.
- [2] D. H. Hodges and E. H. Dowell, (1974 December) *"Nonlinear equations of motion for the elastic bending and torsion of twisted non uniform rotor blades"*, NASA Technical Note.
- [3] P. van der Male, K. N. van Dalen, and A. V. Metrikine, (2016 August) *"The effect of the non-linear velocity and history dependencies of the aerodynamic force on the dynamic response of a rotating wind turbine blade"*, Journal of Sound and Vibration 383, 191.
- [4] J. C. Houbolt and G. W. Brooks, (1957 February) *"Differential equations of the motion for combined flapwise bending, chordwise bending, and torsion of twisted nonuniform rotor blades"*, NACA Technical Note 3905.
- [5] H. Kim, H. H. Yoo, and J. Chung, (2013 July) *"Dynamic model for free vibration and response analysis of rotating beams"*, Journal of Sound and Vibration 332
- [6] G. Surace, V. Anghel, and C. Mares, (1997 April) *"Coupled bending-bending-torsion vibration analysis of rotating pretwisted blades: An integral formulation and numerical examples"*, Journal of Sound and Vibration 206(4), 473.
- [7] S. M. Lin, C. T. Wu, and S. Y. Lee (2003) *"Analysis of rotating nonuniform pretwisted beams with an elastically restrained root and a tip mass"*, International Journal of Mechanical Sciences 45, 741.
- [8] J. Jonkman, S. Butterfield, W. Musial, and G. Scott, (2009) *"Definition of a 5-mw reference wind turbine for offshore system development"*, Technical Report NREL.
- [9] M. O. L. Hansen, (2008) *"Aerodynamics of Wind Turbines, 2nd edition"*, Earthscan, United Kingdom.
- [10] J. M. Gere, (2006) *"Mechanics of Materials, 6th edition"*, Thomson Brooks/Cole.
- [11] M. Géradin and D. J. Rixen, (2015) *"Mechanical Vibrations: Theory and Application to Structural Dynamics, 3rd edition"* Wiley.
- [12] L. Meirovitch, (1980) *"Computational Methods in Structural Dynamics"* Sijthoff & Noordhoff, Alphen aan den Rijn, The Netherlands.
- [13] L. Meirovitch, (2001) *"Fundamentals of Vibrations"* McGraw-Hill, New York, NY 10020.
- [14] Henri P. Gavin, (2015) *"Strain Energy in Linear Elastic Solids"* Department of Civil and Environmental Engineering, Duke University
- [15] K.J Bathe, (2016) *"Finite Element Procedures"* Prentice Hall, Pearson Education, Inc
- [16] Singiresu S. Rao, (2011) *"Mechanical Vibrations"* Prentice Hall, 1 Lake Street, Upper Saddle River, NJ 07458
- [17] David V. Hutton, (2004) *"Fundamentals of Finite Element Analysis"* McGraw-Hill, New York, NY 10020.
- [18] T. Yokoyama, (1988) *"Free vibration characteristics of rotating timoshenko beam,"* International Journal of Mechanical Sciences 30(10), 743.

- [19] M. S. Jeong, I. Lee, S. J. Yoo, and K. C. Park, (2013) "*Torsional stiffness effects on the dynamic stability of a horizontal axis wind turbine blade*," Journal of Renewable and Sustainable Energy 6, 2242.
- [20] M. S. Jeong, M. C. Cha, S. W. Kim, I. Lee, and T. Kim, (2014) "*Effects of torsional degree of freedom, geometric nonlinearity, and gravity on aeroelastic behavior of large-scale horizontal axis wind turbine blades under varying wind speed conditions*," Journal of Renewable and Sustainable Energy 6, 2242.
- [21] Shuangyuan Wang, Yixiang Huang, Lin Li, Chengliang Liu and Daqing Zhang, (2017) "*Dynamic analysis of wind turbines including nacelle-tower-foundation interaction for condition of incomplete structural parameters*" Advances in Mechanical Engineering Vol. 9(3) 1-17.
- [22] Namcheol Kang, Sung Chul Park, Junhong Park and Satya N Atluri, (2016) "*Article Dynamics of flexible tower-blade and rigid nacelle system: dynamic instability due to their interactions in wind turbine*" Journal of Vibration and Control, Vol. 22(3) 826-836.
- [23] S. Kessentini, S. Choura, F. Najjar, M. A Franchek, (2009) "*Modeling and Dynamics of a Horizontal Axis Wind Turbine*" Journal of Vibration and Control, 16(13).
- [24] Tom Irvine, (2012) "*Bending frequencies of beams, rods and pipes*"
- [25] T. Burton, D. Sharpe, N. Jenkins, and E. Bossanyi, (2001) "*Wind energy handbook*" John Wiley & Sons.
- [26] Torbjørn Ruud Hagen, Marit Reiso, Michael Muskulus, (2017) "*Numerical Analysis of Turbulent Flow Past a Truss Tower for Offshore Downwind Turbines*" Department of Civil and Transport Engineering, Norwegian University of Science and Technology Trondheim, Norway.
- [27] Powles, (1983) "*The effect of tower shadow in the dynamics of a horizontal-axis wind turbine*" Wind Engineering, Vol 7, pp 26-42.